

Partial wave analyses of $\psi(3686) \rightarrow p\bar{p}\pi^0$ and $\psi(3686) \rightarrow p\bar{p}\eta$

M. Ablikim¹, M. N. Achasov^{4,c}, P. Adlarson⁷⁶, O. Afedulidis³, X. C. Ai⁸¹, R. Aliberti³⁵, A. Amoroso^{75A,75C}, Q. An^{72,58,a}, Y. Bai⁵⁷, O. Bakina³⁶, I. Balossino^{29A}, Y. Ban^{46,h}, H.-R. Bao⁶⁴, V. Batozskaya^{1,44}, K. Begzsuren³², N. Berger³⁵, M. Berlowski⁴⁴, M. Bertani^{28A}, D. Bettoni^{29A}, F. Bianchi^{75A,75C}, E. Bianco^{75A,75C}, A. Bortone^{75A,75C}, I. Boyko³⁶, R. A. Briere⁵, A. Brueggemann⁶⁹, H. Cai⁷⁷, X. Cai^{1,58}, A. Calcaterra^{28A}, G. F. Cao^{1,64}, N. Cao^{1,64}, S. A. Cetin^{62A}, J. F. Chang^{1,58}, G. R. Che⁴³, G. Chelkov^{36,b}, C. Chen⁴³, C. H. Chen⁹, Chao Chen⁵⁵, G. Chen¹, H. S. Chen^{1,64}, H. Y. Chen²⁰, M. L. Chen^{1,58,64}, S. J. Chen⁴², S. L. Chen⁴⁵, S. M. Chen⁶¹, T. Chen^{1,64}, X. R. Chen^{31,64}, X. T. Chen^{1,64}, Y. B. Chen^{1,58}, Y. Q. Chen³⁴, Z. J. Chen^{25,i}, Z. Y. Chen^{1,64}, S. K. Choi¹⁰, G. Cibinetto^{29A}, F. Cossio^{75C}, J. J. Cui⁵⁰, H. L. Dai^{1,58}, J. P. Dai⁷⁹, A. Dbeyssi¹⁸, R. E. de Boer³, D. Dedovich³⁶, C. Q. Deng⁷³, Z. Y. Deng¹, A. Denig³⁵, I. Denysenko³⁶, M. Destefanis^{75A,75C}, F. De Mori^{75A,75C}, B. Ding^{67,1}, X. X. Ding^{46,h}, Y. Ding³⁴, Y. Ding⁴⁰, J. Dong^{1,58}, L. Y. Dong^{1,64}, M. Y. Dong^{1,58,64}, X. Dong⁷⁷, M. C. Du¹, S. X. Du⁸¹, Y. Y. Duan⁵⁵, Z. H. Duan⁴², P. Egorov^{36,b}, Y. H. Fan⁴⁵, J. Fang⁵⁹, J. Fang^{1,58}, S. S. Fang^{1,64}, W. X. Fang¹, Y. Fang¹, Y. Q. Fang^{1,58}, R. Farinelli^{29A}, L. Fava^{75B,75C}, F. Feldbauer³, G. Felici^{28A}, C. Q. Feng^{72,58}, J. H. Feng⁵⁹, Y. T. Feng^{72,58}, M. Fritsch³, C. D. Fu¹, J. L. Fu⁶⁴, Y. W. Fu^{1,64}, H. Gao⁶⁴, X. B. Gao⁴¹, Y. N. Gao^{46,h}, Yang Gao^{72,58}, S. Garbolino^{75C}, I. Garzia^{29A,29B}, L. Ge⁸¹, P. T. Ge¹⁹, Z. W. Ge⁴², C. Geng⁵⁹, E. M. Gersabeck⁶⁸, A. Gilman⁷⁰, K. Goetzen¹³, L. Gong⁴⁰, W. X. Gong^{1,58}, W. Gradl³⁵, S. Gramigna^{29A,29B}, M. Greco^{75A,75C}, M. H. Gu^{1,58}, Y. T. Gu¹⁵, C. Y. Guan^{1,64}, A. Q. Guo^{31,64}, L. B. Guo⁴¹, M. J. Guo⁵⁰, R. P. Guo⁴⁹, Y. P. Guo^{12,g}, A. Guskov^{36,b}, J. Gutierrez²⁷, K. L. Han⁶⁴, T. T. Han¹, F. Hanisch³, X. Q. Hao¹⁹, F. A. Harris⁶⁶, K. K. He⁵⁵, K. L. He^{1,64}, F. H. Heinsius³, C. H. Heinz³⁵, Y. K. Heng^{1,58,64}, C. Herold⁶⁰, T. Holtmann³, P. C. Hong³⁴, G. Y. Hou^{1,64}, X. T. Hou^{1,64}, Y. R. Hou⁶⁴, Z. L. Hou¹, B. Y. Hu⁵⁹, H. M. Hu^{1,64}, J. F. Hu^{56,j}, S. L. Hu^{12,g}, T. Hu^{1,58,64}, Y. Hu¹, G. S. Huang^{72,58}, K. X. Huang⁵⁹, L. Q. Huang^{31,64}, X. T. Huang⁵⁰, Y. P. Huang¹, Y. S. Huang⁵⁹, T. Hussain⁷⁴, F. Hölzken³, N. Hüsken³⁵, N. in der Wiesche⁶⁹, J. Jackson²⁷, S. Janchiv³², J. H. Jeong¹⁰, Q. Ji¹, Q. P. Ji¹⁹, W. Ji^{1,64}, X. B. Ji^{1,64}, X. L. Ji^{1,58}, Y. Y. Ji⁵⁰, X. Q. Jia⁵⁰, Z. K. Jia^{72,58}, D. Jiang^{1,64}, H. B. Jiang⁷⁷, P. C. Jiang^{46,h}, S. S. Jiang³⁹, T. J. Jiang¹⁶, X. S. Jiang^{1,58,64}, Y. Jiang⁶⁴, J. B. Jiao⁵⁰, J. K. Jiao³⁴, Z. Jiao²³, S. Jin⁴², Y. Jin⁶⁷, M. Q. Jing^{1,64}, X. M. Jing⁶⁴, T. Johansson⁷⁶, S. Kabana³³, N. Kalantar-Nayestanaki⁶⁵, X. L. Kang⁹, X. S. Kang⁴⁰, M. Kavatsyuk⁶⁵, B. C. Ke⁸¹, V. Khachatryan²⁷, A. Khoukaz⁶⁹, R. Kiuchi¹, O. B. Kolcu^{62A}, B. Kopf³, M. Kuessner³, X. Kui^{1,64}, N. Kumar²⁶, A. Kupsc^{44,76}, W. Kühn³⁷, J. J. Lane⁶⁸, L. Lavezzi^{75A,75C}, T. T. Lei^{72,58}, Z. H. Lei^{72,58}, M. Lellmann³⁵, T. Lenz³⁵, C. Li⁴⁷, C. Li⁴³, C. H. Li³⁹, Cheng Li^{72,58}, D. M. Li⁸¹, F. Li^{1,58}, G. Li¹, H. B. Li^{1,64}, H. J. Li¹⁹, H. N. Li^{56,j}, Hui Li⁴³, J. R. Li⁶¹, J. S. Li⁵⁹, K. Li¹, K. L. Li¹⁹, L. J. Li^{1,64}, L. K. Li¹, Lei Li⁴⁸, M. H. Li⁴³, P. R. Li^{38,k,l}, Q. M. Li^{1,64}, Q. X. Li⁵⁰, R. Li^{17,31}, S. X. Li¹², T. Li⁵⁰, W. D. Li^{1,64}, W. G. Li^{1,a}, X. Li^{1,64}, X. H. Li^{72,58}, X. L. Li⁵⁰, X. Y. Li^{1,64}, X. Z. Li⁵⁹, Y. G. Li^{46,h}, Z. J. Li⁵⁹, Z. Y. Li⁷⁹, C. Liang⁴², H. Liang^{1,64}, H. Liang^{72,58}, Y. F. Liang⁵⁴, Y. T. Liang^{31,64}, G. R. Liao¹⁴, Y. P. Liao^{1,64}, J. Libby²⁶, A. Limphirat⁶⁰, C. C. Lin⁵⁵, D. X. Lin^{31,64}, T. Lin¹, B. J. Liu¹, B. X. Liu⁷⁷, C. Liu³⁴, C. X. Liu¹, F. Liu¹, F. H. Liu⁵³, Feng Liu⁶, G. M. Liu^{56,j}, H. Liu^{38,k,l}, H. B. Liu¹⁵, H. H. Liu¹, H. M. Liu^{1,64}, Huihui Liu²¹, J. B. Liu^{72,58}, J. Y. Liu^{1,64}, K. Liu^{38,k,l}, K. Y. Liu⁴⁰, Ke Liu²², L. Liu^{72,58}, L. C. Liu⁴³, Lu Liu⁴³, M. H. Liu^{12,g}, P. L. Liu¹, Q. Liu⁶⁴, S. B. Liu^{72,58}, T. Liu^{12,g}, W. K. Liu⁴³, W. M. Liu^{72,58}, X. Liu³⁹, X. Liu^{38,k,l}, Y. Liu⁸¹, Y. Liu^{38,k,l}, Y. B. Liu⁴³, Z. A. Liu^{1,58,64}, Z. D. Liu⁹, Z. Q. Liu⁵⁰, X. C. Lou^{1,58,64}, F. X. Lu⁵⁹, H. J. Lu²³, J. G. Lu^{1,58}, X. L. Lu¹, Y. Lu⁷, Y. P. Lu^{1,58}, Z. H. Lu^{1,64}, C. L. Luo⁴¹, J. R. Luo⁵⁹, M. X. Luo⁸⁰, T. Luo^{12,g}, X. L. Luo^{1,58}, X. R. Lyu⁶⁴, Y. F. Lyu⁴³, F. C. Ma⁴⁰, H. Ma⁷⁹, H. L. Ma¹, J. L. Ma^{1,64}, L. L. Ma⁵⁰, L. R. Ma⁶⁷, M. M. Ma^{1,64}, Q. M. Ma¹, R. Q. Ma^{1,64}, T. Ma^{72,58}, X. T. Ma^{1,64}, X. Y. Ma^{1,58}, Y. Ma^{46,h}, Y. M. Ma³¹, F. E. Maas¹⁸, M. Maggiora^{75A,75C}, S. Malde⁷⁰, Q. A. Malik⁷⁴, Y. J. Mao^{46,h}, Z. P. Mao¹, S. Marcello^{75A,75C}, Z. X. Meng⁶⁷, J. G. Messchendorp^{13,65}, G. Mezzadri^{29A}, H. Miao^{1,64}, T. J. Min⁴², R. E. Mitchell²⁷, X. H. Mo^{1,58,64}, B. Moses²⁷, N. Yu. Muchnoi^{4,c}, J. Muskalla³⁵, Y. Nefedov³⁶, F. Nerling^{18,e}, L. S. Nie²⁰, I. B. Nikolaev^{4,c}, Z. Ning^{1,58}, S. Nisar^{11,m}, Q. L. Niu^{38,k,l}, W. D. Niu⁵⁵, Y. Niu⁵⁰, S. L. Olsen⁶⁴, Q. Ouyang^{1,58,64}, S. Pacetti^{28B,28C}, X. Pan⁵⁵, Y. Pan⁵⁷, A. Pathak³⁴, Y. P. Pei^{72,58}, M. Pelizaeus³, H. P. Peng^{72,58}, Y. Y. Peng^{38,k,l}, K. Peters^{13,e}, J. L. Ping⁴¹, R. G. Ping^{1,64}, S. Plura³⁵, V. Prasad³³, F. Z. Qi¹, H. Qi^{72,58}, H. R. Qi⁶¹, M. Qi⁴², T. Y. Qi^{12,g}, S. Qian^{1,58}, W. B. Qian⁶⁴, C. F. Qiao⁶⁴, X. K. Qiao⁸¹, J. J. Qin⁷³, L. Q. Qin¹⁴, L. Y. Qin^{72,58}, X. P. Qin^{12,g}, X. S. Qin⁵⁰, Z. H. Qin^{1,58}, J. F. Qiu¹, Z. H. Qu⁷³, C. F. Redmer³⁵, K. J. Ren³⁹, A. Rivetti^{75C}, M. Rolo^{75C}, G. Rong^{1,64}, Ch. Rosner¹⁸, S. N. Ruan⁴³, N. Salone⁴⁴, A. Sarantsev^{36,d}, Y. Schelhaas³⁵, K. Schoenning⁷⁶, M. Scodeggio^{29A}, K. Y. Shan^{12,g}, W. Shan²⁴, X. Y. Shan^{72,58}, Z. J. Shang^{38,k,l}, J. F. Shangguan¹⁶, L. G. Shao^{1,64}, M. Shao^{72,58}, C. P. Shen^{12,g}, H. F. Shen^{1,8}, W. H. Shen⁶⁴, X. Y. Shen^{1,64}, B. A. Shi⁶⁴, H. Shi^{72,58}, H. C. Shi^{72,58}, J. L. Shi^{12,g}, J. Y. Shi¹, Q. Q. Shi⁵⁵, S. Y. Shi⁷³, X. Shi^{1,58}, J. J. Song¹⁹, T. Z. Song⁵⁹, W. M. Song^{34,1}, Y. J. Song^{12,g}, Y. X. Song^{46,h,n}, S. Sosio^{75A,75C}, S. Spataro^{75A,75C}, F. Stieler³⁵,

S. S. Su⁴⁰, Y. J. Su⁶⁴, G. B. Sun⁷⁷, G. X. Sun¹, H. Sun⁶⁴, H. K. Sun¹, J. F. Sun¹⁹, K. Sun⁶¹, L. Sun⁷⁷, S. S. Sun^{1,64}, T. Sun^{51,f}, W. Y. Sun³⁴, Y. Sun⁹, Y. J. Sun^{72,58}, Y. Z. Sun¹, Z. Q. Sun^{1,64}, Z. T. Sun⁵⁰, C. J. Tang⁵⁴, G. Y. Tang¹, J. Tang⁵⁹, M. Tang^{72,58}, Y. A. Tang⁷⁷, L. Y. Tao⁷³, Q. T. Tao^{25,i}, M. Tat⁷⁰, J. X. Teng^{72,58}, V. Thoren⁷⁶, W. H. Tian⁵⁹, Y. Tian^{31,64}, Z. F. Tian⁷⁷, I. Uman^{62B}, Y. Wan⁵⁵, S. J. Wang⁵⁰, B. Wang¹, B. L. Wang⁶⁴, Bo Wang^{72,58}, D. Y. Wang^{46,h}, F. Wang⁷³, H. J. Wang^{38,k,l}, J. J. Wang⁷⁷, J. P. Wang⁵⁰, K. Wang^{1,58}, L. L. Wang¹, M. Wang⁵⁰, N. Y. Wang⁶⁴, S. Wang^{12,g}, S. Wang^{38,k,l}, T. Wang^{12,g}, T. J. Wang⁴³, W. Wang⁷³, W. Wang⁵⁹, W. P. Wang^{35,58,72,o}, X. Wang^{46,h}, X. F. Wang^{38,k,l}, X. J. Wang³⁹, X. L. Wang^{12,g}, X. N. Wang¹, Y. Wang⁶¹, Y. D. Wang⁴⁵, Y. F. Wang^{1,58,64}, Y. L. Wang¹⁹, Y. N. Wang⁴⁵, Y. Q. Wang¹, Yaqian Wang¹⁷, Yi Wang⁶¹, Z. Wang^{1,58}, Z. L. Wang⁷³, Z. Y. Wang^{1,64}, Ziyi Wang⁶⁴, D. H. Wei¹⁴, F. Weidner⁶⁹, S. P. Wen¹, Y. R. Wen³⁹, U. Wiedner³, G. Wilkinson⁷⁰, M. Wolke⁷⁶, L. Wollenberg³, C. Wu³⁹, J. F. Wu^{1,8}, L. H. Wu¹, L. J. Wu^{1,64}, X. Wu^{12,g}, X. H. Wu³⁴, Y. Wu^{72,58}, Y. H. Wu⁵⁵, Y. J. Wu³¹, Z. Wu^{1,58}, L. Xia^{72,58}, X. M. Xian³⁹, B. H. Xiang^{1,64}, T. Xiang^{46,h}, D. Xiao^{38,k,l}, G. Y. Xiao⁴², S. Y. Xiao¹, Y. L. Xiao^{12,g}, Z. J. Xiao⁴¹, C. Xie⁴², X. H. Xie^{46,h}, Y. Xie⁵⁰, Y. G. Xie^{1,58}, Y. H. Xie⁶, Z. P. Xie^{72,58}, T. Y. Xing^{1,64}, C. F. Xu^{1,64}, C. J. Xu⁵⁹, G. F. Xu¹, H. Y. Xu^{67,2,p}, M. Xu^{72,58}, Q. J. Xu¹⁶, Q. N. Xu³⁰, W. Xu¹, W. L. Xu⁶⁷, X. P. Xu⁵⁵, Y. Xu⁴⁰, Y. C. Xu⁷⁸, Z. S. Xu⁶⁴, F. Yan^{12,g}, L. Yan^{12,g}, W. B. Yan^{72,58}, W. C. Yan⁸¹, X. Q. Yan^{1,64}, H. J. Yang^{51,f}, H. L. Yang³⁴, H. X. Yang¹, T. Yang¹, Y. Yang^{12,g}, Y. F. Yang^{1,64}, Y. F. Yang⁴³, Y. X. Yang^{1,64}, Z. W. Yang^{38,k,l}, Z. P. Yao⁵⁰, M. Ye^{1,58}, M. H. Ye⁸, J. H. Yin¹, Junhao Yin⁴³, Z. Y. You⁵⁹, B. X. Yu^{1,58,64}, C. X. Yu⁴³, G. Yu^{1,64}, J. S. Yu^{25,i}, M. C. Yu⁴⁰, T. Yu⁷³, X. D. Yu^{46,h}, Y. C. Yu⁸¹, C. Z. Yuan^{1,64}, J. Yuan³⁴, J. Yuan⁴⁵, L. Yuan², S. C. Yuan^{1,64}, Y. Yuan^{1,64}, Z. Y. Yuan⁵⁹, C. X. Yue³⁹, A. A. Zafar⁷⁴, F. R. Zeng⁵⁰, S. H. Zeng^{63A,63B,63C,63D}, X. Zeng^{12,g}, Y. Zeng^{25,i}, Y. J. Zeng⁵⁹, Y. J. Zeng^{1,64}, X. Y. Zhai³⁴, Y. C. Zhai⁵⁰, Y. H. Zhan⁵⁹, A. Q. Zhang^{1,64}, B. L. Zhang^{1,64}, B. X. Zhang¹, D. H. Zhang⁴³, G. Y. Zhang¹⁹, H. Zhang⁸¹, H. Zhang^{72,58}, H. C. Zhang^{1,58,64}, H. H. Zhang⁵⁹, H. H. Zhang³⁴, H. Q. Zhang^{1,58,64}, H. R. Zhang^{72,58}, H. Y. Zhang^{1,58}, J. Zhang⁸¹, J. Zhang⁵⁹, J. J. Zhang⁵², J. L. Zhang²⁰, J. Q. Zhang⁴¹, J. S. Zhang^{12,g}, J. W. Zhang^{1,58,64}, J. X. Zhang^{38,k,l}, J. Y. Zhang¹, J. Z. Zhang^{1,64}, Jianyu Zhang⁶⁴, L. M. Zhang⁶¹, Lei Zhang⁴², P. Zhang^{1,64}, Q. Y. Zhang³⁴, R. Y. Zhang^{38,k,l}, S. H. Zhang^{1,64}, Shulei Zhang^{25,i}, X. D. Zhang⁴⁵, X. M. Zhang¹, X. Y. Zhang⁴⁰, X. Y. Zhang⁵⁰, Y. Zhang⁷³, Y. Zhang¹, Y. T. Zhang⁸¹, Y. H. Zhang^{1,58}, Y. M. Zhang³⁹, Yan Zhang^{72,58}, Z. D. Zhang¹, Z. H. Zhang¹, Z. L. Zhang³⁴, Z. Y. Zhang⁷⁷, Z. Y. Zhang⁴³, Z. Z. Zhang⁴⁵, G. Zhao¹, J. Y. Zhao^{1,64}, J. Z. Zhao^{1,58}, L. Zhao¹, Lei Zhao^{72,58}, M. G. Zhao⁴³, N. Zhao⁷⁹, R. P. Zhao⁶⁴, S. J. Zhao⁸¹, Y. B. Zhao^{1,58}, Y. X. Zhao^{31,64}, Z. G. Zhao^{72,58}, A. Zhemchugov^{36,b}, B. Zheng⁷³, B. M. Zheng³⁴, J. P. Zheng^{1,58}, W. J. Zheng^{1,64}, Y. H. Zheng⁶⁴, B. Zhong⁴¹, X. Zhong⁵⁹, H. Zhou⁵⁰, J. Y. Zhou³⁴, L. P. Zhou^{1,64}, S. Zhou⁶, X. Zhou⁷⁷, X. K. Zhou⁶, X. R. Zhou^{72,58}, X. Y. Zhou³⁹, Y. Z. Zhou^{12,g}, Z. C. Zhou²⁰, A. N. Zhu⁶⁴, J. Zhu⁴³, K. Zhu¹, K. J. Zhu^{1,58,64}, K. S. Zhu^{12,g}, L. Zhu³⁴, L. X. Zhu⁶⁴, S. H. Zhu⁷¹, T. J. Zhu^{12,g}, W. D. Zhu⁴¹, Y. C. Zhu^{72,58}, Z. A. Zhu^{1,64}, J. H. Zou¹, J. Zu^{72,58}

(BESIII Collaboration)

¹ *Institute of High Energy Physics, Beijing 100049, People's Republic of China*

² *Beihang University, Beijing 100191, People's Republic of China*

³ *Bochum Ruhr-University, D-44780 Bochum, Germany*

⁴ *Budker Institute of Nuclear Physics SB RAS (BINP), Novosibirsk 630090, Russia*

⁵ *Carnegie Mellon University, Pittsburgh, Pennsylvania 15213, USA*

⁶ *Central China Normal University, Wuhan 430079, People's Republic of China*

⁷ *Central South University, Changsha 410083, People's Republic of China*

⁸ *China Center of Advanced Science and Technology, Beijing 100190, People's Republic of China*

⁹ *China University of Geosciences, Wuhan 430074, People's Republic of China*

¹⁰ *Chung-Ang University, Seoul, 06974, Republic of Korea*

¹¹ *COMSATS University Islamabad, Lahore Campus, Defence Road, Off Raiwind Road, 54000 Lahore, Pakistan*

¹² *Fudan University, Shanghai 200433, People's Republic of China*

¹³ *GSI Helmholtzcentre for Heavy Ion Research GmbH, D-64291 Darmstadt, Germany*

¹⁴ *Guangxi Normal University, Guilin 541004, People's Republic of China*

¹⁵ *Guangxi University, Nanning 530004, People's Republic of China*

¹⁶ *Hangzhou Normal University, Hangzhou 310036, People's Republic of China*

¹⁷ *Hebei University, Baoding 071002, People's Republic of China*

¹⁸ *Helmholtz Institute Mainz, Staudinger Weg 18, D-55099 Mainz, Germany*

¹⁹ *Henan Normal University, Xinxiang 453007, People's Republic of China*

²⁰ *Henan University, Kaifeng 475004, People's Republic of China*

- ²¹ Henan University of Science and Technology, Luoyang 471003, People's Republic of China
- ²² Henan University of Technology, Zhengzhou 450001, People's Republic of China
- ²³ Huangshan College, Huangshan 245000, People's Republic of China
- ²⁴ Hunan Normal University, Changsha 410081, People's Republic of China
- ²⁵ Hunan University, Changsha 410082, People's Republic of China
- ²⁶ Indian Institute of Technology Madras, Chennai 600036, India
- ²⁷ Indiana University, Bloomington, Indiana 47405, USA
- ²⁸ INFN Laboratori Nazionali di Frascati , (A)INFN Laboratori Nazionali di Frascati, I-00044, Frascati, Italy; (B)INFN Sezione di Perugia, I-06100, Perugia, Italy; (C)University of Perugia, I-06100, Perugia, Italy
- ²⁹ INFN Sezione di Ferrara, (A)INFN Sezione di Ferrara, I-44122, Ferrara, Italy; (B)University of Ferrara, I-44122, Ferrara, Italy
- ³⁰ Inner Mongolia University, Hohhot 010021, People's Republic of China
- ³¹ Institute of Modern Physics, Lanzhou 730000, People's Republic of China
- ³² Institute of Physics and Technology, Peace Avenue 54B, Ulaanbaatar 13330, Mongolia
- ³³ Instituto de Alta Investigación, Universidad de Tarapacá, Casilla 7D, Arica 1000000, Chile
- ³⁴ Jilin University, Changchun 130012, People's Republic of China
- ³⁵ Johannes Gutenberg University of Mainz, Johann-Joachim-Becher-Weg 45, D-55099 Mainz, Germany
- ³⁶ Joint Institute for Nuclear Research, 141980 Dubna, Moscow region, Russia
- ³⁷ Justus-Liebig-Universität Giessen, II. Physikalisches Institut, Heinrich-Buff-Ring 16, D-35392 Giessen, Germany
- ³⁸ Lanzhou University, Lanzhou 730000, People's Republic of China
- ³⁹ Liaoning Normal University, Dalian 116029, People's Republic of China
- ⁴⁰ Liaoning University, Shenyang 110036, People's Republic of China
- ⁴¹ Nanjing Normal University, Nanjing 210023, People's Republic of China
- ⁴² Nanjing University, Nanjing 210093, People's Republic of China
- ⁴³ Nankai University, Tianjin 300071, People's Republic of China
- ⁴⁴ National Centre for Nuclear Research, Warsaw 02-093, Poland
- ⁴⁵ North China Electric Power University, Beijing 102206, People's Republic of China
- ⁴⁶ Peking University, Beijing 100871, People's Republic of China
- ⁴⁷ Qufu Normal University, Qufu 273165, People's Republic of China
- ⁴⁸ Renmin University of China, Beijing 100872, People's Republic of China
- ⁴⁹ Shandong Normal University, Jinan 250014, People's Republic of China
- ⁵⁰ Shandong University, Jinan 250100, People's Republic of China
- ⁵¹ Shanghai Jiao Tong University, Shanghai 200240, People's Republic of China
- ⁵² Shanxi Normal University, Linfen 041004, People's Republic of China
- ⁵³ Shanxi University, Taiyuan 030006, People's Republic of China
- ⁵⁴ Sichuan University, Chengdu 610064, People's Republic of China
- ⁵⁵ Soochow University, Suzhou 215006, People's Republic of China
- ⁵⁶ South China Normal University, Guangzhou 510006, People's Republic of China
- ⁵⁷ Southeast University, Nanjing 211100, People's Republic of China
- ⁵⁸ State Key Laboratory of Particle Detection and Electronics, Beijing 100049, Hefei 230026, People's Republic of China
- ⁵⁹ Sun Yat-Sen University, Guangzhou 510275, People's Republic of China
- ⁶⁰ Suranaree University of Technology, University Avenue 111, Nakhon Ratchasima 30000, Thailand
- ⁶¹ Tsinghua University, Beijing 100084, People's Republic of China
- ⁶² Turkish Accelerator Center Particle Factory Group, (A)Istinye University, 34010, Istanbul, Turkey; (B)Near East University, Nicosia, North Cyprus, 99138, Mersin 10, Turkey
- ⁶³ University of Bristol, (A)H H Wills Physics Laboratory; (B)Tyndall Avenue; (C)Bristol; (D)BS8 1TL
- ⁶⁴ University of Chinese Academy of Sciences, Beijing 100049, People's Republic of China
- ⁶⁵ University of Groningen, NL-9747 AA Groningen, The Netherlands
- ⁶⁶ University of Hawaii, Honolulu, Hawaii 96822, USA
- ⁶⁷ University of Jinan, Jinan 250022, People's Republic of China
- ⁶⁸ University of Manchester, Oxford Road, Manchester, M13 9PL, United Kingdom
- ⁶⁹ University of Muenster, Wilhelm-Klemm-Strasse 9, 48149 Muenster, Germany

⁷⁰ *University of Oxford, Keble Road, Oxford OX13RH, United Kingdom*

⁷¹ *University of Science and Technology Liaoning, Anshan 114051, People's Republic of China*

⁷² *University of Science and Technology of China, Hefei 230026, People's Republic of China*

⁷³ *University of South China, Hengyang 421001, People's Republic of China*

⁷⁴ *University of the Punjab, Lahore-54590, Pakistan*

⁷⁵ *University of Turin and INFN, (A)University of Turin, I-10125, Turin, Italy; (B)University of Eastern Piedmont, I-15121, Alessandria, Italy; (C)INFN, I-10125, Turin, Italy*

⁷⁶ *Uppsala University, Box 516, SE-75120 Uppsala, Sweden*

⁷⁷ *Wuhan University, Wuhan 430072, People's Republic of China*

⁷⁸ *Yantai University, Yantai 264005, People's Republic of China*

⁷⁹ *Yunnan University, Kunming 650500, People's Republic of China*

⁸⁰ *Zhejiang University, Hangzhou 310027, People's Republic of China*

⁸¹ *Zhengzhou University, Zhengzhou 450001, People's Republic of China*

^a *Deceased*

^b *Also at the Moscow Institute of Physics and Technology, Moscow 141700, Russia*

^c *Also at the Novosibirsk State University, Novosibirsk, 630090, Russia*

^d *Also at the NRC "Kurchatov Institute", PNPI, 188300, Gatchina, Russia*

^e *Also at Goethe University Frankfurt, 60323 Frankfurt am Main, Germany*

^f *Also at Key Laboratory for Particle Physics, Astrophysics and Cosmology, Ministry of Education; Shanghai Key Laboratory for Particle Physics and Cosmology; Institute of Nuclear and Particle Physics, Shanghai 200240, People's Republic of China*

^g *Also at Key Laboratory of Nuclear Physics and Ion-beam Application (MOE) and Institute of Modern Physics, Fudan University, Shanghai 200443, People's Republic of China*

^h *Also at State Key Laboratory of Nuclear Physics and Technology, Peking University, Beijing 100871, People's Republic of China*

ⁱ *Also at School of Physics and Electronics, Hunan University, Changsha 410082, China*

^j *Also at Guangdong Provincial Key Laboratory of Nuclear Science, Institute of Quantum Matter, South China Normal University, Guangzhou 510006, China*

^k *Also at MOE Frontiers Science Center for Rare Isotopes,*

Lanzhou University, Lanzhou 730000, People's Republic of China

^l *Also at Lanzhou Center for Theoretical Physics, Lanzhou University, Lanzhou 730000, People's Republic of China*

^m *Also at the Department of Mathematical Sciences, IBA, Karachi 75270, Pakistan*

ⁿ *Also at Ecole Polytechnique Federale de Lausanne (EPFL), CH-1015 Lausanne, Switzerland*

^o *Also at Helmholtz Institute Mainz, Staudinger Weg 18, D-55099 Mainz, Germany*

^p *Also at School of Physics, Beihang University, Beijing 100191, China*

Using a sample of $(2712 \pm 14) \times 10^6$ $\psi(3686)$ events collected with the BESIII detector, we perform partial wave analyses of the decays $\psi(3686) \rightarrow p\bar{p}\pi^0$ and $\psi(3686) \rightarrow p\bar{p}\eta$. The branching fractions of $\psi(3686) \rightarrow p\bar{p}\pi^0$ and $\psi(3686) \rightarrow p\bar{p}\eta$ are determined to be $(133.9 \pm 11.2 \pm 2.3) \times 10^{-6}$ or $(183.7 \pm 13.7 \pm 3.2) \times 10^{-6}$ and $(61.5 \pm 6.5 \pm 1.1) \times 10^{-6}$ or $(84.4 \pm 6.9 \pm 1.4) \times 10^{-6}$, respectively, where the two solutions are caused by an ambiguous phase angle between resonant and continuum processes. Several well-established N^* states are observed in the $p\pi^0$ and $p\eta$ systems, and the corresponding branching fractions are measured. The ratio of decay widths $\Gamma_{N(1535) \rightarrow N\eta} / \Gamma_{N(1535) \rightarrow N\pi}$ is determined to be $0.99 \pm 0.05 \pm 0.19$.

I. INTRODUCTION

The nature of the lowest lying $J^P = 1/2^-$ nucleon resonance $N(1535)$ is not well understood as of yet. According to the conventional constituent quark model, the mass of the first orbital angular momentum excitation state, $N(1535)$, should always be below that of the first radial excitation state, $N(1440)$ [1], also known as the Roper resonance. However, the experimental results indicate that the $N(1535)$ has a mass higher than $N(1440)$

by around 100 MeV, which has been a puzzle for several decades. Meanwhile, the measured partial width of $N(1535) \rightarrow N\eta$ is much larger than expectation. An estimation based on flavor symmetry predicts a ratio of $\frac{\Gamma_{N(1535) \rightarrow N\eta}}{\Gamma_{N(1535) \rightarrow N\pi^0}} = 0.17$ [2]. However, results from various multi-channel partial wave analyses (PWAs) in fixed-target experiments listed by the Particle Data Group (PDG) [3] suggest an average value of 1.00 ± 0.40 , which deviates from the prediction by 2σ but suffers from poor

precision.

Several theoretical studies have attempted to pin down the nature of $N(1535)$, explaining its mass puzzle and strong coupling to the η meson [1]. Some investigations [4–6] suggest that $N(1535)$ is a dynamically generated quasi-bound state in the $K\Lambda$ and $K\Sigma$ channels, thus containing a sizable $s\bar{s}$ admixture. In some other investigations [7–9], the $N(1535)$ is assumed to have a penta-quark $uuds\bar{s}$ component. For these two scenarios, the assumption of five-quark contribution gives a natural explanation for the larger mass and enhanced coupling to $N\eta$ of $N(1535)$. Additionally, a study [10] based on lattice QCD suggests a scenario where a three-quark core is dominating.

Experimentally, the decays of $\psi(3686) \rightarrow p\bar{p}\pi^0$ and $\psi(3686) \rightarrow p\bar{p}\eta$ have previously been studied by the CLEO and BESIII Collaborations. With 2.45×10^7 $\psi(3686)$ events, the CLEO collaboration reported evidence for several excited N^* states in the $p\pi^0$ system in $\psi(3686) \rightarrow p\bar{p}\pi^0$ and in the $p\eta$ system in $\psi(3686) \rightarrow p\bar{p}\eta$ decays [11]. Later, using 1.06×10^8 $\psi(3686)$ events collected in 2009, BESIII reported on PWAs of $\psi(3686) \rightarrow p\bar{p}\pi^0$ [12] and $\psi(3686) \rightarrow p\bar{p}\eta$ [13], respectively. A ratio of decay widths $\frac{\Gamma_{N(1535) \rightarrow N\eta}}{\Gamma_{N(1535) \rightarrow N\pi^0}} = 0.70 \pm 0.09^{+0.52}_{-0.32}$ was obtained with large systematic uncertainty, and no conclusion can be drawn from this measurement. An improved measurement of this ratio is expected to strongly constrain the parameter space of the $N(1535)$, and hence to draw a firm conclusion on its deviation from flavor symmetry and pin down its nature.

The BESIII experiment has collected $(2712 \pm 14) \times 10^6$ $\psi(3686)$ events, which provides an excellent opportunity to explore the nature of the $N(1535)$. In this article, we present PWAs of the decays $\psi(3686) \rightarrow p\bar{p}\pi^0$ and $\psi(3686) \rightarrow p\bar{p}\eta$ based on the full $\psi(3686)$ sample.

II. DETECTOR AND DATA SAMPLES

The BESIII detector [14] records symmetric e^+e^- collisions provided by the BEPCII storage ring [15] in the center-of-mass energy (\sqrt{s}) range from 2.0 to 4.95 GeV, with a peak luminosity of $1.1 \times 10^{33} \text{ cm}^{-2}\text{s}^{-1}$ achieved at $\sqrt{s} = 3.77$ GeV. BESIII has collected large data samples in this energy region [16–18]. The cylindrical core of the BESIII detector covers 93% of the full solid angle and consists of a helium-based multilayer drift chamber (MDC), a plastic scintillator time-of-flight system (TOF), and a CsI(Tl) electromagnetic calorimeter (EMC), which are all enclosed in a superconducting solenoidal magnet providing a 1.0 T magnetic field. The solenoid is supported by an octagonal flux-return yoke with resistive plate counter muon identification modules interleaved with steel. The charged-particle momentum resolution at 1 GeV/ c is 0.5%, and the specific energy loss (dE/dx) resolution is 6% for electrons from Bhabha scattering. The EMC measures photon energies with a

resolution of 2.5% (5%) at 1 GeV in the barrel (end cap) region. The time resolution in the TOF barrel region is 68 ps, while that in the end cap region was 110 ps. The end cap TOF system was upgraded in 2015 using multigap resistive plate chamber technology, providing a time resolution of 60 ps [19]. The data sample taken in 2021, about 83% of the total data set used in this paper, benefits from this upgrade.

Monte Carlo (MC) simulated data samples produced with a GEANT4-based [20] software package, which includes the geometric description of the BESIII detector and the detector response, are used to determine detection efficiencies and to estimate backgrounds. The simulation models the beam energy spread and initial state radiation (ISR) in the e^+e^- annihilations with the generator KKMC [21]. The ‘inclusive’ MC sample includes the production of the $\psi(3686)$ resonance, the ISR production of the J/ψ , and the continuum processes incorporated in KKMC [21]. All particle decays are modeled with EVTGEN [22] using branching fractions either taken from the PDG [3], when available, or otherwise estimated with LUNDCHARM [23]. To take into account the efficiency and luminosity difference between various rounds of data taking, both the exclusive and inclusive MC samples are simulated in different rounds separately, and then mixed together according to corresponding integrated luminosity.

III. EVENT SELECTION AND BACKGROUND STUDY

Candidates for $\psi(3686) \rightarrow p\bar{p}\pi^0, \pi^0 \rightarrow \gamma\gamma$ and $\psi(3686) \rightarrow p\bar{p}\eta, \eta \rightarrow \gamma\gamma$ are required to have two charged tracks with opposite charge and at least two photon candidates. The charged tracks are required to satisfy $|V_z| < 10$ cm, $V_r < 1$ cm, and $|\cos\theta| < 0.93$. Here, $|V_z|$ and V_r are the distances of the point of closest approach to the interaction point of the reconstructed track in the z direction and the transverse (x - y) plane, respectively, and θ is the polar angle of charged track defined with respect to the z axis. The z axis is defined as the symmetry axis of the MDC. Photon candidates are reconstructed from isolated clusters in the EMC. Their energies are required to be greater than 25 MeV in the barrel ($|\cos\theta| < 0.8$) and 50 MeV in the end cap ($0.86 < |\cos\theta| < 0.92$) regions. Clusters caused by electronic noise or beam backgrounds are suppressed by requiring the cluster time to be within [0, 700] ns after the event start time. To suppress fake photons produced by hadronic interactions in the EMC and secondary photons from bremsstrahlung, clusters within a cone of 20° around the extrapolated position in the EMC of any charged track are rejected.

To suppress the combinatorial background and improve the resolution, a five-constraint (5C) kinematic fit for the $\psi(3686) \rightarrow p\bar{p}\gamma\gamma$ hypothesis is performed, where in addition to overall energy-momentum conservation, the invariant mass of the two photons is constrained to

the known mass of π^0 or η . The combination with the minimum χ_{5C}^2 is kept for further analysis. The χ_{5C}^2 of the kinematic fit is required to be smaller than 30. The background from $J/\psi \rightarrow p\bar{p}$ is suppressed by rejecting events with $|M_{p\bar{p}} - 3.097| < 0.050$ GeV, where $M_{p\bar{p}}$ is the $p\bar{p}$ invariant mass.

A total of 190,729 candidates for $\psi(3686) \rightarrow p\bar{p}\pi^0$ and 31,441 candidates for $\psi(3686) \rightarrow p\bar{p}\eta$ satisfy the above selection criteria. Dalitz plots are shown in Fig. 1, in which several excited N^* states and $p\bar{p}$ structures can be seen. Studies of the $\psi(3686)$ inclusive MC sample indicate that the total background fraction $\frac{B}{S+B}$ from $\psi(3686)$ decays is 6.4% for $\psi(3686) \rightarrow p\bar{p}\pi^0$, dominated by $\psi(3686) \rightarrow p\bar{p}\gamma^{\text{FSR}}$ and K/π misidentified as protons. For $\psi(3686) \rightarrow p\bar{p}\eta$, the background fraction is 9.5%, and the dominant background contributions are from $\psi(3686) \rightarrow \gamma\chi_{cJ}$ with $\chi_{cJ} \rightarrow p\bar{p}\pi^0, p\bar{p}\gamma^{\text{FSR}}$, where γ^{FSR} is the final state radiation photon.

To estimate the contribution from the continuum processes $e^+e^- \rightarrow p\bar{p}\pi^0$ and $e^+e^- \rightarrow p\bar{p}\eta$, exactly the same selection criteria as above are applied to a data sample at $\sqrt{s} = 3.773$ GeV with an integrated luminosity of $\mathcal{L} = 2.93$ fb $^{-1}$. No evidence of $\psi(3770) \rightarrow p\bar{p}\pi^0$ is observed [38] with current statistics; therefore this data sample is assumed to be dominated by the continuum process.

The interference between $\psi(3686)$ resonance and continuum process is studied by using the $\psi(3686)$ scan data samples collected from $\sqrt{s} = 3.670$ to 3.710 GeV with a total integrated luminosity $\mathcal{L} = 417.7$ pb $^{-1}$. The charged tracks of the $p\bar{p}\eta$ final state are selected with the same criteria as above, while additional particle identification (PID) by using TOF and MDC dE/dx information is imposed to the $p\bar{p}\pi^0$ final state to suppress peaking background. A charged track is identified as a proton if its PID confidence level for the proton hypothesis is larger than that for the pion and kaon hypotheses. The selection for photon candidates is kept to be the same as for the $\psi(3686)$ data sample. A four-momentum constraint (4C) kinematic fit is performed and the corresponding χ_{4C}^2 is required to be less than 30. The veto on the $J/\psi \rightarrow p\bar{p}$ background is also applied.

IV. PARTIAL WAVE ANALYSIS

A. Amplitude

In the PWA, the decay amplitudes for the sequential decays, via an intermediate states of a neutral meson M^0 or charged $N^{*\pm}$,

$$\begin{aligned} \psi(3686) &\rightarrow M^0\pi^0(\eta), M^0 \rightarrow p\bar{p}, \\ \psi(3686) &\rightarrow N^{*+}\bar{p}, N^{*+} \rightarrow p\pi^0(\eta), \\ \psi(3686) &\rightarrow \bar{N}^{*-}p, \bar{N}^{*-} \rightarrow \bar{p}\pi^0(\eta), \end{aligned} \quad (1)$$

are constructed using the relativistic covariant tensor amplitude formalism [24]. The structure for the baryon-antibaryon-meson vertices is composed by $p_i^\mu, \gamma_\mu, g^{\mu\nu}, \epsilon^{\alpha\beta\rho\sigma}$ and their products or contractions, where p_i are the momenta of the particles involved. These effective vertices are deduced from an effective Lagrangian

$$\mathcal{L} = \bar{\psi}_1\Gamma\psi_2A, \quad (2)$$

where Γ is the effective vertex, and $\psi_{1,2}$ and A are the baryon and virtual photon fields, respectively. Here, the Lorentz indices are omitted. For the strong decays considered in this work (Eq. 1), the corresponding interaction Lagrangian must be C- and P-parity invariant, Lorentz invariant, and CPT invariant. These constraints lead to the strong interaction vertices satisfying

$$\Gamma = \xi_A C(\gamma_0\Gamma^+\gamma_0)^T C^{-1} \text{ and } \Gamma = \eta_1\eta_2\eta_A\gamma_0\Gamma^P\gamma_0, \quad (3)$$

where ξ_A is the C parity of the virtual photon; $C = -i\gamma_2\gamma_0$ is the C transformation operator; Γ^+ is the Hermitian conjugation of Γ ; η_A and $\eta_{1,2}$ are the P parities of meson and baryons, respectively; Γ^P is the vertex Γ after P-parity transformation.

The amplitude \mathcal{A}_j of a decay via a resonance is

$$\mathcal{A}_j = \epsilon^{*\alpha}(p_0, m)\bar{u}(p_1, s_1)\Gamma_{1\alpha\mu_1\mu_2\dots}\Gamma_2^{\mu_1\mu_2\dots}v(p_2, s_2)\text{BW}(s), \quad (4)$$

where ϵ^* is the $\psi(3686)$ polarization vector; $u(p_1, s_1)$ and $v(p_2, s_2)$ are the free Dirac spinors for proton and anti-proton, respectively; Γ_1 and Γ_2 are the strong interaction vertices for the resonances with $\psi(3686)$ and p, \bar{p} and π^0 or η ; $\text{BW}(s)$ is a Breit-Wigner function.

The decay dynamics of the three lowest lying N^* states are described with the KSU model [25]. The energy-dependent Breit-Wigner width is parametrized as

$$\Gamma(\sqrt{s'}) = \Gamma_0 \times \sum_i r_i \times \frac{\rho_i(\sqrt{s'})}{\rho_i(m_0)}, \quad (5)$$

where $\sqrt{s'}$ is the two-body invariant mass of $p\pi^0$ or $p\eta$, m_0 is the mass of N^* , and r_i is the branching fraction of the i -th decay channel of N^* as summarized in Table 1. For the two-body decay of a resonance into the

Table 1. The dominant decay channels and corresponding branching fractions of the three lowest lying N^* in unit of percent [25].

Resonance	$N(1440)$		$N(1520)$		$N(1535)$	
Decay	$N\pi$	60 ± 2	$N\pi$	59 ± 2	$N\pi$	43 ± 2
	$\Delta\pi$	23 ± 4	$\Delta\pi(\text{S-wave})$	21 ± 2	$N\eta$	43 ± 2
	$N\sigma$	17 ± 3	$\Delta\pi(\text{D-wave})$	6 ± 1	$N\rho$	14 ± 2
	—	—	$N\rho$	14 ± 2	—	—

i -th channel with two stable particles, the phase-space

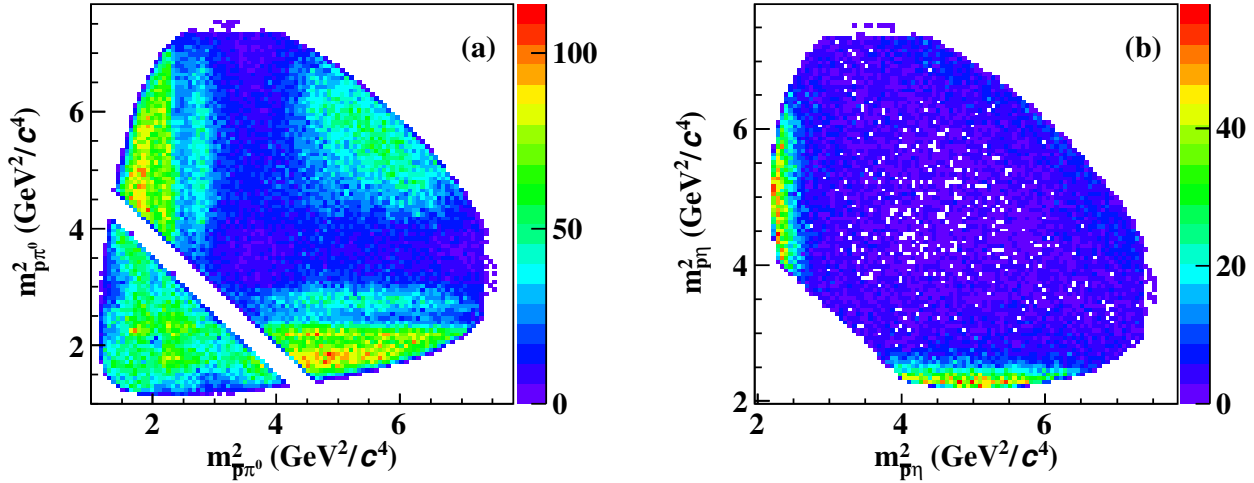


Fig. 1. Dalitz plots of the selected (a) $\psi(3686) \rightarrow p\bar{p}\pi^0$ and (b) $\psi(3686) \rightarrow p\bar{p}\eta$ candidates from data.

factor is parametrized as

$$\rho_i = \frac{q_i}{\sqrt{s'}} \times B_l^2(q_i R), \quad (6)$$

where q_i is the momentum of the two particles in their center-of-mass frame, B_{l_i} is the Blatt-Weisskopf barrier penetration factor [26], and l_i is the orbital angular momentum of the two particles. The range parameter R is fixed at 0.73 fm. The first three Blatt-Weisskopf factors are given as

$$\begin{aligned} B_0^2(x) &= 1, \\ B_1^2(x) &= \frac{x^2}{1+x^2}, \\ B_2^2(x) &= \frac{x^4}{9+3x^2+x^4}, \end{aligned} \quad (7)$$

where $x = q_i R$. For a quasi-two-body decay of a resonance into the i -th channel consisting of a stable particle of mass m and an isobar of mass M , which is assumed to decay into stable particles with masses m_1 and m_2 , the phase-space factor is calculated numerically by

$$\rho_i = \int_{m_1+m_2}^{\sqrt{s'}-m} \frac{q}{\sqrt{s'}} \times B_l^2(qR) \times BW'(M) \times dM. \quad (8)$$

Here $BW'(M)$ is the line shape of the isobar, which is parametrized by a Breit-Wigner function with a constant width, E791 type [27], and the Gounaris-Sakurai model [28] for Δ , σ , and ρ , respectively. For the other intermediate states, the constant width $\Gamma(m) = \Gamma_0$ is used. In the fit, all the masses and widths are fixed to the central values shown in Table 2.

B. Fit method

The complex coupling constants of the amplitudes are determined by an unbinned maximum likelihood fit. The probability to observe the i -th event characterized by ξ_i , *i.e.*, the measured four momenta of the particles in the final state, is

$$p(\xi_i) = \frac{\omega(\xi_i)\epsilon(\xi_i)}{\int d\Phi \omega(\xi)\epsilon(\xi)}, \quad (9)$$

where $\omega(\xi_i) \equiv (\frac{d\sigma}{d\Phi})_i$ is the differential cross section, ϵ is the detection efficiency, $d\Phi$ is the standard element of phase space for the three-body decays and $\sigma' = \int d\Phi \omega(\xi)\epsilon(\xi)$ is the observed total cross section. The differential cross section is

$$\omega(\xi) \equiv \frac{d\sigma}{d\Phi} = \left| \sum_j A_j \right|^2, \quad (10)$$

where A_j is the amplitude for the j -th resonance.

The likelihood for the data sample is taken as

$$\mathcal{L} = \prod_{i=1}^N P(\xi_i) = \prod_{i=1}^N \frac{\omega(\xi_i)\epsilon(\xi_i)}{\sigma'}. \quad (11)$$

Technically, the MINUIT package [29] is used to minimize a negative log-likelihood (NLL) function, $\mathcal{S} = -\ln \mathcal{L}$, instead of maximizing \mathcal{L} , with

$$\mathcal{S} = -\ln \mathcal{L} = -\sum_i \ln \left[\frac{\omega(\xi_i)}{\sigma'} \right] - \sum_i \ln \epsilon(\xi_i). \quad (12)$$

In Eq. 12, the second term is independent on the pa-

parameters and has no impact on the determination of the parameters or on the relative changes in \mathcal{S} . In the fit, $-\ln \mathcal{L}$ is reduced to

$$\mathcal{S} = -\sum_i^N \ln \omega(\xi_i) + N \ln \sigma'. \quad (13)$$

The observed total cross section σ' is evaluated using an MC sample consisting of N_{gen} signal events distributed uniformly in phase space. These events are subjected to the selection criteria described in Sec. III and yield a sample of N_{acc} accepted events. The normalization integral is then computed as

$$\int d\Phi \omega(\xi) \epsilon(\xi) = \sigma' = \frac{1}{N_{\text{gen}}} \sum_k^{N_{\text{acc}}} \omega(\xi_k). \quad (14)$$

The background contribution in the fit is estimated using the inclusive MC sample and is subtracted from the $-\ln \mathcal{L}$ function by

$$\mathcal{S} = -(\ln \mathcal{L}_{\text{data}} - \ln \mathcal{L}_{\text{bkg}}). \quad (15)$$

After the parameters are determined in the fit, the signal yield of a given resonance is estimated by scaling its cross section ratio r_j to the net number of events

$$N_j = r_j (N_{\text{data}} - N_{\text{bkg}}), \quad \text{with } r_j = \frac{\sigma'_j}{\sigma'}, \quad (16)$$

where $\sigma'_j = \int d\Phi \omega_j(\xi) \epsilon(\xi)$ is the observed cross section for the j -th resonance with $\omega_j = |\mathcal{A}_j|^2$, N_{data} is the number of observed events in data and N_{bkg} is the number of background events.

The statistical uncertainty of the signal yield N_i , δN_i , is estimated according to the uncertainty propagation formula using the covariance matrix obtained in the fit.

C. Amplitude analysis results of $\psi(3686) \rightarrow p\bar{p}\pi^0$

A PWA is performed to the selected 190,729 candidate events for $\psi(3686) \rightarrow p\bar{p}\pi^0$, where the background yield is determined to be 12,172 with the inclusive MC sample.

The N^* states with $J < \frac{5}{2}$ and certain existence of $N^* \rightarrow N\pi$ from the PDG [3], *i.e.* $N(1440)$, $N(1520)$, $N(1535)$, $N(1710)$, and $N(1720)$, are considered in the significance test. Additionally, the $N(2100)$, $N(2300)$, and $N(2570)$ are included according to the previous studies on $J/\psi \rightarrow p\bar{n}\pi^- + c.c.$ [30] and $\psi(3686) \rightarrow p\bar{p}\pi^0$ [12]. According to the framework of soft π meson theory [32], an off shell process $N(940) \rightarrow p\pi^0$ is included. The significant contribution from the virtual proton pole $N(940)$ is expected [31] and also observed by several experiment studies [12, 30, 33]. Thus, $N(940)$ is also included into significance test. The $p\bar{p}$ structures are explained with $\rho(1900)$ [34], $\rho(2000)$ [35], $\rho(2150)$ [36], and $\rho(2225)$ [37].

The statistical significance of those intermediate states are estimated by removing one of them from solution at one time. Based on changes in the log-likelihood and the number of degrees of freedom, the statistical significance is calculated. All intermediate states yield significance greater than 5σ , thus are kept in the baseline solution. Table 2 shows the resonance parameters and quantum numbers of those intermediate states.

Figure 2 shows the projections of PWA fit result on the two-body invariant mass spectra $M_{p\pi^0}$, $M_{\bar{p}\pi^0}$, and $M_{p\bar{p}}$, respectively. The fit result gives a good description of the data sample. The fitted signal yields of N^* states at $\sqrt{s} = 3.686$ GeV, denoted as N_{sig} , are summarized in Table 3.

The contribution from the continuum process is studied by performing the same PWA fit to the data sample at $\sqrt{s} = 3.773$ GeV, as shown in Fig. 3. The fitted signal yields of N^* states at $\sqrt{s} = 3.773$ GeV, denoted as N_{con} , are also summarized in Table 3. Potential contributions from the isospin violating processes $\gamma^* \rightarrow (\omega/\phi)^* \pi^0$ are tested and found to be insignificant. Considering the significant contribution of ρ^* states from continuum process and potential strong interference between $\psi(3686)$ resonance and continuum production, only the branching fractions of N^* states are reported. The yield N_{con} is further rescaled to $\sqrt{s} = 3.686$ GeV with the factor

$$f_c = \frac{\mathcal{L}^{3686} \times \sigma_{\text{Born}}^{3686} \times (\epsilon(1+\delta))^{3686}}{\mathcal{L}^{3773} \times \sigma_{\text{Born}}^{3773} \times (\epsilon(1+\delta))^{3773}} \quad (17)$$

by considering the integrated luminosity \mathcal{L} , Born cross section σ_{Born} , efficiency ϵ , and initial state radiation (ISR) correction $(1+\delta)$. The integrated luminosities at $\sqrt{s} = 3.686$ GeV and $\sqrt{s} = 3.773$ GeV are 4.08 fb^{-1} and 2.93 fb^{-1} , respectively. The Born cross sections of $e^+e^- \rightarrow p\bar{p}\pi^0$ are estimated with Ref. [38]. The efficiency is obtained by generating MC samples with the PWA fit result at $\sqrt{s} = 3.773$ GeV. The radiative correction factor $(1+\delta)$ is given by CONEXC [39] based on the Born cross section. The f_c is determined to be 1.564.

The net signal yield is obtained by subtracting the normalized contribution from the continuum process, denoted as N_{net} , and is calculated with $N_{\text{net}} = N_{\text{sig}} - f_c \times N_{\text{con}}$. The signal efficiency ϵ for each intermediate state is obtained from a generated corresponding signal MC sample according to the PWA fit result at $\sqrt{s} = 3.686$ GeV. The branching fractions are given by

$$\mathcal{B} = \frac{N_{\text{net}}}{\epsilon \times \mathcal{B}(\pi^0 \rightarrow \gamma\gamma) \times N_{\psi(3686)}}, \quad (18)$$

as summarized in Table 3. Compared to the previous study on $\psi(3686) \rightarrow p\bar{p}\pi^0$ [12], there are some mild tensions, which are attributed mainly to differences in the treatment of continuum backgrounds in the PWA and several newly-included ρ^* and N^* states in the baseline solution.

Table 2. The resonance parameters, quantum numbers, and references of intermediate states involved in the baseline solutions $\psi(3686) \rightarrow p\bar{p}\pi^0$ and $\psi(3686) \rightarrow p\bar{p}\eta$.

Resonance state	Mass (MeV/ c^2)	Width (MeV)	$I^G(J^{PC})$	comment
$\rho(1900)$	1880 ± 30	130 ± 30	$1^+(1^{--})$	Ref. [34]
$\rho(2000)$	2078 ± 6	149 ± 21	$1^+(1^{--})$	Ref. [35]
$\rho(2150)$	2254 ± 22	109 ± 76	$1^+(1^{--})$	Ref. [36]
$\rho(2225)$	2225 ± 35	335 ± 100	$1^+(2^{--})$	Ref. [37]
$\phi_3(1850)$	1854 ± 7	87 ± 28	$0^-(3^{--})$	PDG [3]
$\omega(1960)$	1960 ± 25	195 ± 60	$0^-(1^{--})$	Ref. [40]
$\omega(2205)$	2205 ± 30	350 ± 90	$0^-(1^{--})$	Ref. [40]
$N(940)$	940	0	$\frac{1}{2}(\frac{1}{2}^+)$	Virtual proton pole
$N(1440)$	1406 ± 3	314 ± 9	$\frac{1}{2}(\frac{1}{2}^+)$	Optimized with data
$N(1520)$	1512 ± 2	121 ± 3	$\frac{1}{2}(\frac{3}{2}^-)$	Ref. [25]
$N(1535)$	1525 ± 2	147 ± 5	$\frac{1}{2}(\frac{1}{2}^-)$	Ref. [25]
$N(1650)$	1666 ± 3	133 ± 7	$\frac{1}{2}(\frac{1}{2}^-)$	Ref. [25]
$N(1710)$	1710 ± 30	140 ± 60	$\frac{1}{2}(\frac{1}{2}^+)$	PDG [3]
$N(1720)$	1720 ± 30	250 ± 100	$\frac{1}{2}(\frac{3}{2}^+)$	PDG [3]
$N(1895)$	1895 ± 25	120 ± 80	$\frac{1}{2}(\frac{1}{2}^-)$	PDG [3]
$N(2100)$	2100 ± 50	260 ± 60	$\frac{1}{2}(\frac{1}{2}^+)$	PDG [3]
$N(2300)$	2300 ± 116	340 ± 114	$\frac{1}{2}(\frac{1}{2}^+)$	PDG [3]
$N(2570)$	2570 ± 39	250 ± 70	$\frac{1}{2}(\frac{5}{2}^-)$	PDG [3]

Table 3. Numbers used to calculate branching fractions of N^* states in $\psi(3686) \rightarrow p\bar{p}\pi^0$. N_{sig} is the fitted yield from PWA of $\psi(3686)$ data sample. N_{con} is the fitted yield from PWA of continuum data sample. N_{net} is the net signal yield calculated with $N_{\text{net}} = N_{\text{sig}} - f_c \times N_{\text{con}}$, where f_c is the normalization factor, ϵ is signal efficiency and \mathcal{B} is branching fraction. Here, first uncertainties are statistical and the second are systematic.

Resonance state	N_{sig}	N_{con}	N_{net}	ϵ (%)	\mathcal{B} ($\times 10^{-6}$)
$N(940)$	122215 ± 3266	656 ± 164	121188 ± 3276	39.71	$113.9 \pm 3.1 \pm 11.9$
$N(1440)$	57118 ± 1383	953 ± 147	55627 ± 1402	38.34	$54.2 \pm 1.4 \pm 14.1$
$N(1520)$	8109 ± 428	870 ± 81	6749 ± 446	38.43	$6.6 \pm 0.4 \pm 2.0$
$N(1535)$	18894 ± 778	240 ± 77	18519 ± 787	39.61	$17.5 \pm 0.7 \pm 3.6$
$N(1650)$	11146 ± 794	278 ± 79	10712 ± 804	43.75	$9.1 \pm 0.7 \pm 3.2$
$N(1710)$	5043 ± 472	369 ± 100	4466 ± 497	39.73	$4.2 \pm 0.5 \pm 4.0$
$N(1720)$	6983 ± 523	217 ± 83	6644 ± 539	39.93	$6.2 \pm 0.5 \pm 2.4$
$N(2100)$	11107 ± 1033	551 ± 161	10245 ± 1063	44.90	$8.5 \pm 0.9 \pm 3.8$
$N(2300)$	5633 ± 566	894 ± 222	4235 ± 664	43.75	$3.6 \pm 0.6 \pm 3.0$
$N(2570)$	27716 ± 1041	2349 ± 187	24043 ± 1082	46.14	$19.5 \pm 0.9 \pm 14.5$

D. Amplitude analysis results of $\psi(3686) \rightarrow p\bar{p}\eta$

A PWA is performed to the selected 31,441 candidate events for $\psi(3686) \rightarrow p\bar{p}\eta$, where the background yield is determined to be 2,986 with the inclusive MC sample.

The N^* states with at least fair existence of $N^* \rightarrow N\eta$ from the PDG [3], *i.e.* $N(1535)$, $N(1650)$, $N(1710)$, and $N(1895)$, are considered in the significance test. The $N(1520)$ is not included since the $\Gamma_{N\eta}/\Gamma_{\text{tot}}$ is smaller than 1% for this resonance. The $p\bar{p}$ structures are explained with several excited ω and ϕ states. The statistical significance of all N^* states and some of the structures in $p\bar{p}$, $\phi_3(1850)$, $\omega(1960)$ [40], and $\omega(2205)$ [40] are greater

than 5σ , hence they are kept in the baseline solution. The contribution from the virtual proton pole $N(940)$ in the $p\bar{p}\eta$ final state is expected to be negligible [32] and also found to be insignificant in the PWA fit. Table 2 shows the resonance parameters and quantum numbers of those intermediate states.

Figure 4 shows the projection of PWA result on the two-body invariant mass spectra $M_{p\eta}$, $M_{\bar{p}\eta}$, and $M_{p\bar{p}}$, respectively. The distribution of data sample is well described by the fit result.

The same study as described above in Sec. IV C to estimate the continuum contribution is performed. The results are shown in Fig. 5. Based on the Born cross sections of $e^+e^- \rightarrow p\bar{p}\eta$ taken from Ref. [41], the nor-

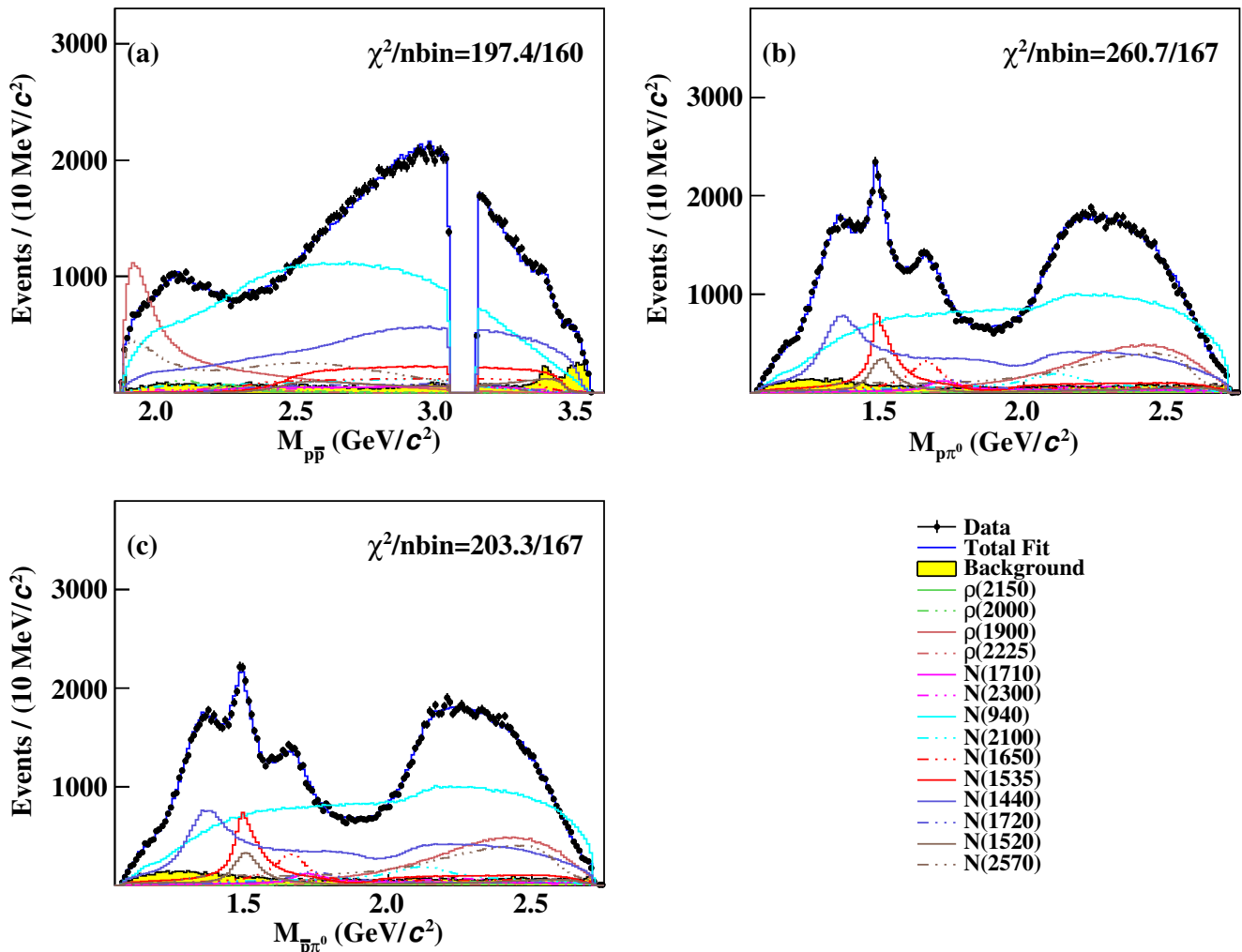


Fig. 2. Projections of the PWA fit at $\sqrt{s} = 3.686$ GeV on the (a) $p\bar{p}$, (b) $p\pi^0$, and (c) $\bar{p}\pi^0$ invariant mass distributions. The points with errors are data, the blue curves are the fit result, the curves in various colors denote different resonant components and the yellow filled histograms are the simulated background.

malization factor f_c is determined to be 1.623 according to Eq. 17. The parameters N_{sig} , N_{con} , N_{net} , and ϵ for $\psi(3686) \rightarrow p\bar{p}\eta$ have exactly the same definition as in Sec. IV C. The branching fractions are given with

$$\mathcal{B} = \frac{N_{\text{net}}}{\epsilon \times \mathcal{B}(\eta \rightarrow \gamma\gamma) \times N_{\psi(3686)}}, \quad (19)$$

and summarized in Table 4. For $N(1650)$ and $N(1895)$, the N_{net} value are consistent with zero within two times the statistical uncertainties; the corresponding branching fractions are not reported. The determined branching fraction of $N(1535)$ is in good agreement with the previous measurement [13].

V. OBSERVED CROSS SECTION

The branching fractions of $\psi(3686) \rightarrow p\bar{p}\pi^0$ and $\psi(3686) \rightarrow p\bar{p}\eta$ is determined by fitting the observed cross sections at nine energy points around the $\psi(3686)$ peak, including both the $\psi(3686)$ data sample and the $\psi(3686)$ -scan data sample. Here, the $\psi(3686)$ data sample is selected in the same way as that of scan data sample.

The signal yield N_{obs} at each energy point is determined by a fit to the $m_{\gamma\gamma}$ spectrum. The signal shape is described with the MC simulated shape convolved with a Gaussian function to take into account the resolution difference between data and MC simulation. The background shape is parametrized as a linear function. As an example, Fig. 6 shows the fit results to the selected candidates of the $\psi(3686)$ data sample.

The detection efficiency is determined with the sig-

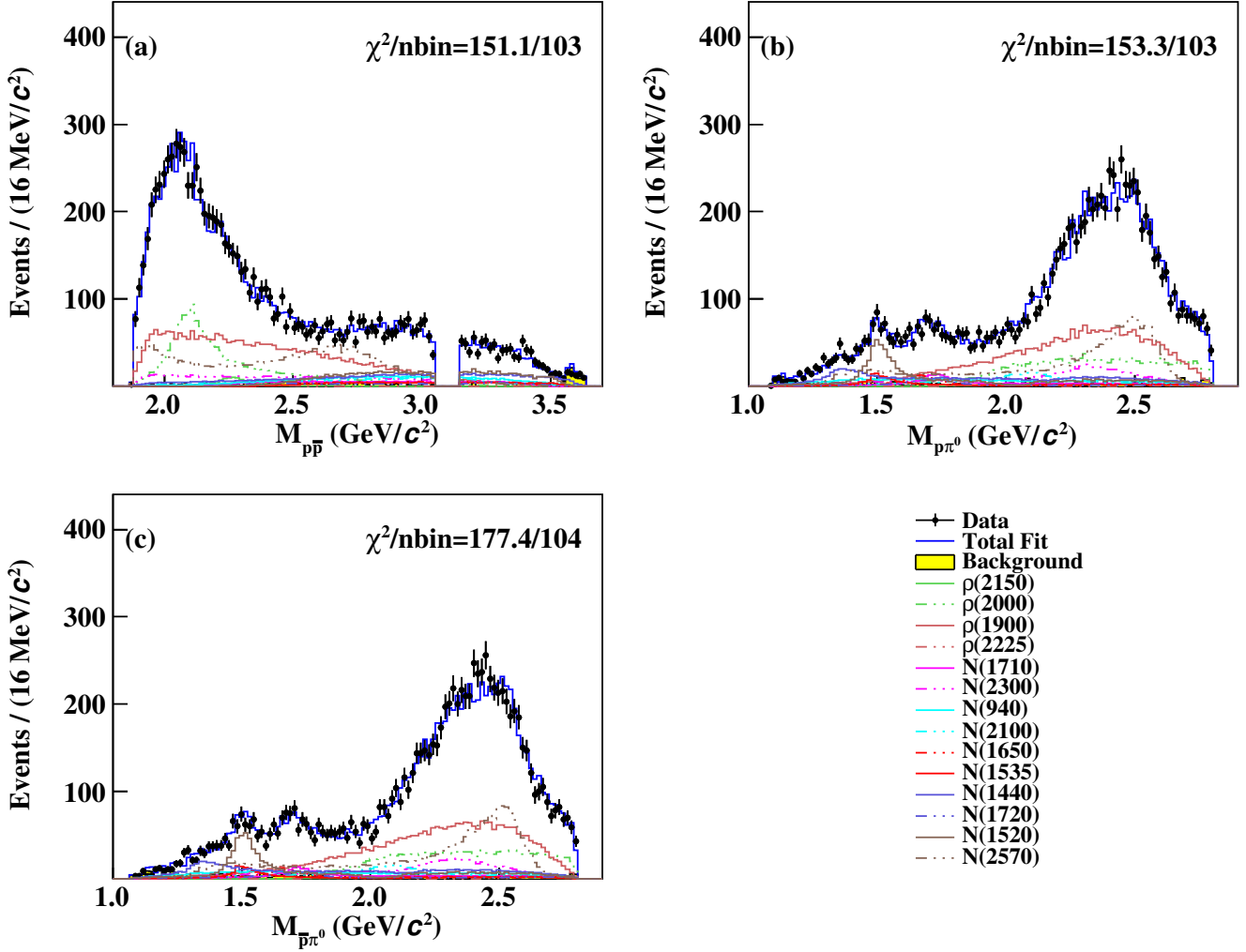


Fig. 3. Projections of the PWA fit at $\sqrt{s} = 3.773$ GeV on the (a) $p\bar{p}$, (b) $p\pi^0$, and (c) $\bar{p}\pi^0$ invariant mass distributions. The points with errors are data, the blue curves are the fit result, the curves in various colors denote different resonant components and the yellow filled histograms are the simulated background.

Table 4. Numbers used to calculate branching fractions of N^* states in $\psi(3686) \rightarrow p\bar{p}\eta$. The definition is exactly the same as that of Table 3. Here, the first uncertainties are statistical and the second are systematic.

Resonance state	N_{sig}	N_{con}	N_{net}	ϵ (%)	$\mathcal{B} (\times 10^{-6})$
$N(1535)$	20411 ± 460	570 ± 115	19486 ± 486	36.17	$50.5 \pm 1.3 \pm 7.1$
$N(1650)$	809 ± 310	388 ± 88	180 ± 341	—	—
$N(1710)$	3351 ± 273	63 ± 63	3250 ± 292	38.81	$7.8 \pm 0.7 \pm 3.1$
$N(1895)$	198 ± 50	71 ± 32	83 ± 72	—	—

nal MC samples generated based on the PWA results at $\sqrt{s} = 3.686$ GeV and 3.773 GeV. The ISR effect is included with CONEXC, which depends on the Born cross sections as input. Therefore, several rounds of iteration are performed. First, the signal MC samples are generated by using the Born cross sections with continuum process only. Then, the detection efficiency ϵ is obtained

and the observed cross section σ_{obs} is calculated with

$$\sigma_{\text{obs}} = \frac{N_{\text{obs}}}{\mathcal{L}_{\text{int}} \times \epsilon \times \mathcal{B}(\pi^0(\eta) \rightarrow \gamma\gamma)}. \quad (20)$$

Next, a fit is performed to the energy-dependent observed cross sections with statistical uncertainty only. The detail of the fit is described in Sec. VII. The fitted line shape of the cross sections is used as the input to gener-

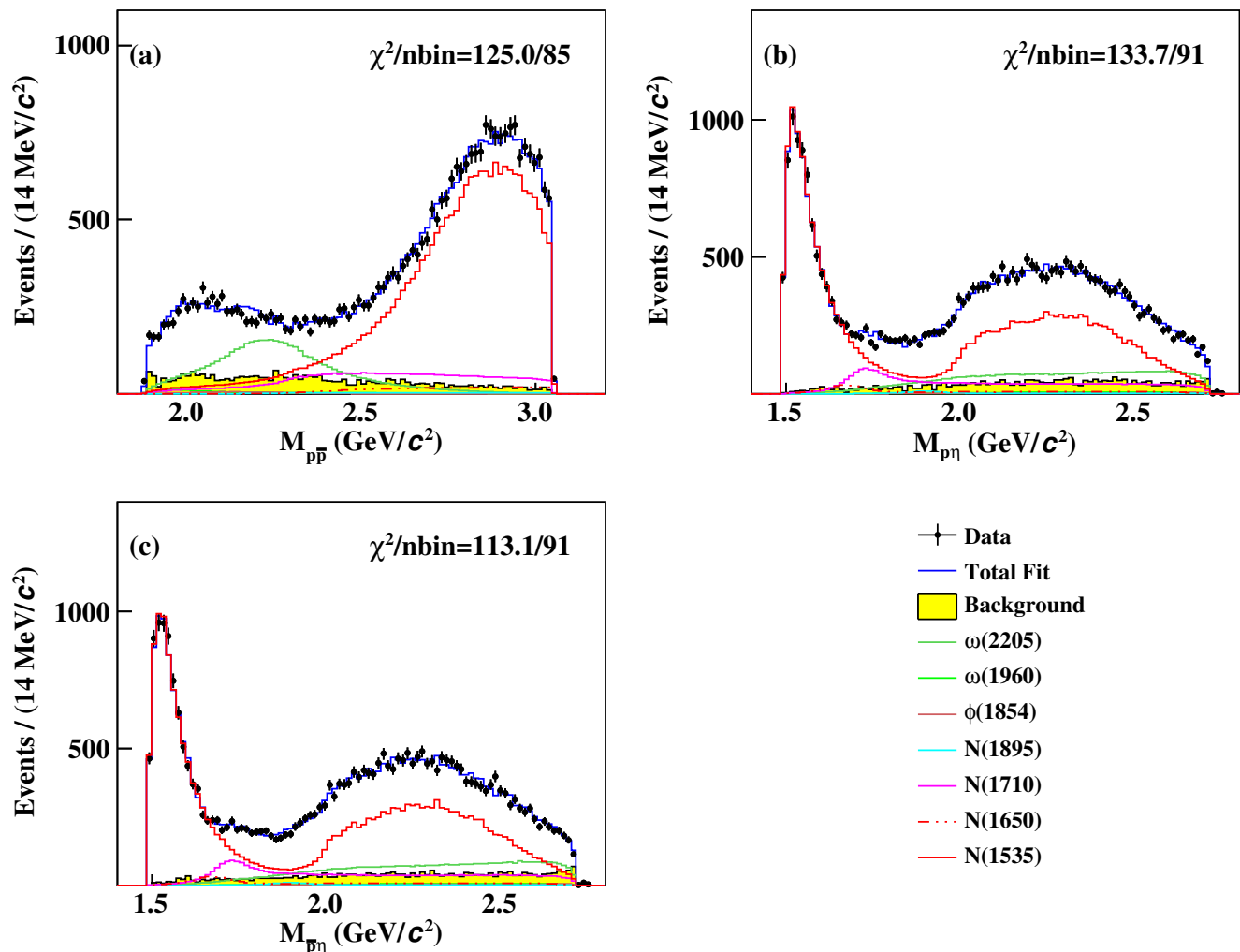


Fig. 4. Projections of the PWA fit at $\sqrt{s} = 3.686$ GeV on the (a) $p\bar{p}$, (b) $p\eta$, and (c) $\bar{p}\eta$ invariant mass distributions. The points with errors are data, the blue curves are the fit result, the curves in various colors denote different resonant components and the yellow filled histograms are the simulated background.

ate signal MC samples in the next iteration. The process is repeated until the result is stable. Table 5 shows the obtained observed cross sections.

VI. SYSTEMATIC UNCERTAINTIES

A. Uncertainties on observed cross sections

The systematic uncertainties on the observed cross section measurement include several sources, as summarized in Table 6. They are estimated as described below.

The integrated luminosity is measured using Bhabha scattering events, with an uncertainty less than 1.0% [42]. The uncertainty related to tracking efficiency of proton is estimated to be 1.0% using a control sample of $J/\psi \rightarrow p\pi^-\bar{p}\pi^+$ [43]. The uncertainty due to the PID efficiency is

studied with a control sample of $J/\psi \rightarrow pK^-\bar{\Lambda} + c.c.$ [43], which is taken to be 1.0% for proton and 2.0% for anti-proton, respectively. The uncertainty from photon detection is taken to be 1.0% per photon [44].

The systematic uncertainty due to the J/ψ veto requirement is estimated by varying the cut range within [0.044, 0.056] GeV with a step size of 0.002 GeV. The difference between the average of re-measured branching fractions with varied cuts and nominal value is taken to be the uncertainty. The systematic uncertainty associated with the kinematic fit is estimated by performing corrections on the track helix parameter in the MC simulation [45]. The difference between the detection efficiencies obtained with and without the helix parameter correction is taken as the corresponding systematic uncertainty.

The systematic uncertainty of MC modeling is estimated with a new signal MC sample, in which all fitted

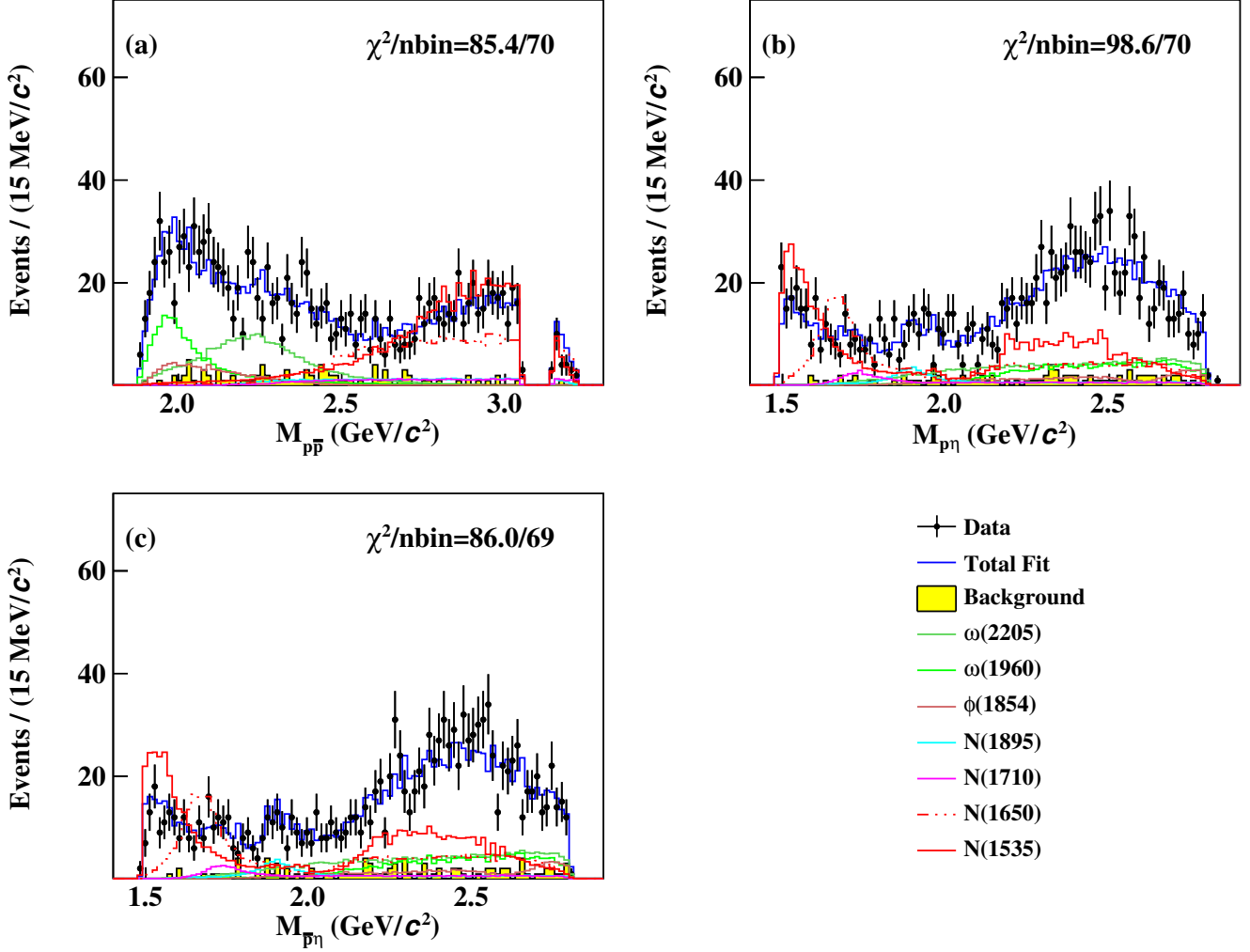


Fig. 5. Projections of the PWA fit at $\sqrt{s} = 3.773$ GeV on the (a) $p\bar{p}$, (b) $p\eta$, and (c) $\bar{p}\eta$ invariant mass distributions. The points with errors are data, the blue curves are the fit result, the curves in various colors denote different resonant components and the yellow filled histograms are the simulated background.

Table 5. The measured observed cross sections of $e^+e^- \rightarrow p\bar{p}\pi^0$ and $e^+e^- \rightarrow p\bar{p}\eta$ around the $\psi(3686)$ peak. Here, \mathcal{L} is the integrated luminosity; N_{sig} is the number of observed signal event; ϵ is the detection efficiency; The uncertainties are statistical only.

\sqrt{s} (MeV)	\mathcal{L} (pb $^{-1}$)	$N_{\text{sig}}^{\pi^0}$	ϵ^{π^0} (%)	$\sigma_{\text{obs}}^{\pi^0}$ (pb)	N_{sig}^{η}	ϵ^{η} (%)	$\sigma_{\text{obs}}^{\eta}$ (pb)
3670.16	84.7	294 ± 18	43.47	8.1 ± 0.5	55 ± 8	40.96	4.0 ± 0.6
3680.14	84.8	257 ± 17	42.56	7.2 ± 0.5	41 ± 7	40.30	3.0 ± 0.5
3682.75	28.7	122 ± 12	40.46	10.7 ± 1.0	25 ± 6	39.63	5.6 ± 1.2
3684.22	28.7	431 ± 21	38.42	39.6 ± 1.9	96 ± 12	39.55	21.4 ± 2.5
3685.26	26.0	984 ± 33	38.55	99.4 ± 3.2	173 ± 15	39.65	42.6 ± 3.7
3686.10	3877.1	183914 ± 441	38.51	124.7 ± 0.3	29920 ± 205	39.67	49.4 ± 0.3
3686.50	25.1	1104 ± 34	38.51	115.5 ± 3.5	201 ± 18	39.60	51.3 ± 4.4
3691.36	69.4	504 ± 23	40.40	18.2 ± 0.8	86 ± 11	39.49	8.0 ± 1.0
3709.76	70.3	294 ± 18	38.29	11.1 ± 0.6	49 ± 8	36.72	4.8 ± 0.7

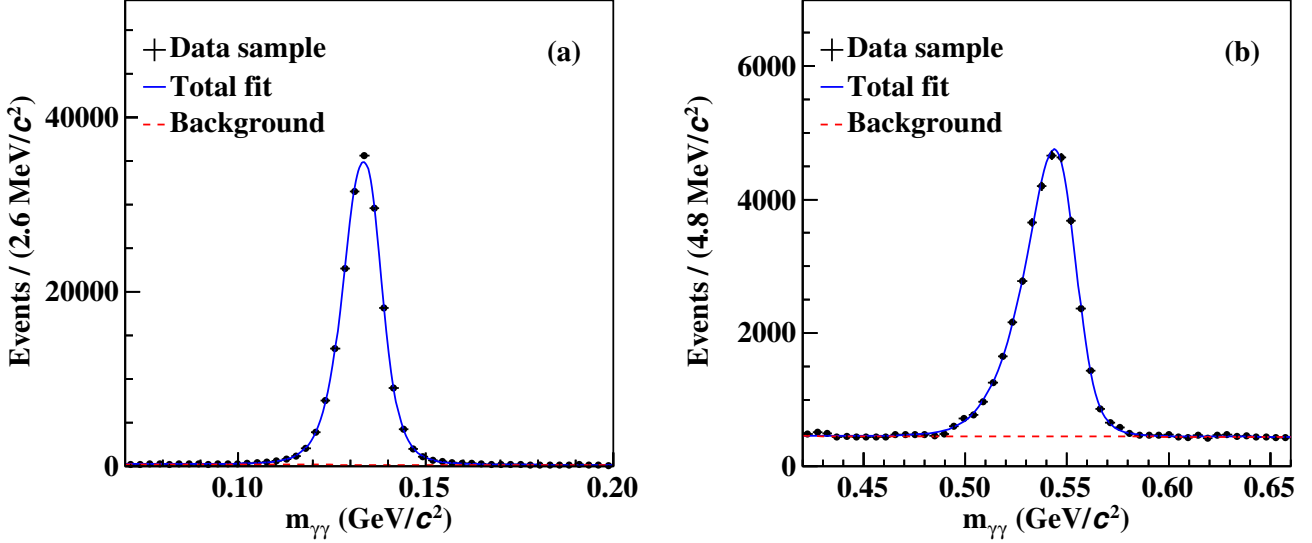


Fig. 6. Fits to the $m_{\gamma\gamma}$ spectra of the selected candidates of the $\psi(3686)$ data sample in (a) π^0 and (b) η signal zones. The points with errors are the $\psi(3686)$ data, the blue solid curves are the fit results, and the red dashed curves are the background contributions.

Table 6. Systematic uncertainties on the measurement of observed cross sections of $\psi(3686) \rightarrow p\bar{p}\pi^0$ and $\psi(3686) \rightarrow p\bar{p}\eta$ in unit of percent.

$\psi(3686) \rightarrow p\bar{p}\pi^0$	3670.16	3680.14	3682.75	3684.22	3685.26	3686.10	3686.50	3691.36	3709.76
Photon detection	2.0								
PID of proton	3.0								
Tracking	2.0								
Luminosity	1.0								
Helix parameter	0.8	0.5	0.7	0.5	0.6	0.5	0.5	0.6	0.9
Peaking background	0.3								
J/ψ veto	0.2	0.4	0.5	0.3	0.1	< 0.1	0.1	0.3	0.1
$\mathcal{B}(\pi^0 \rightarrow \gamma\gamma)$	< 0.1								
MC modeling	0.4	0.3	0.2	0.2	0.6	0.2	0.3	0.2	0.1
Fit to $m_{\gamma\gamma}$	1.1	0.2	0.2	0.7	0.2	0.4	0.4	0.4	0.6
Total	4.5	4.3	4.3	4.4	4.3	4.3	4.3	4.3	4.4
$\psi(3686) \rightarrow p\bar{p}\eta$	3670.16	3680.14	3682.75	3684.22	3685.26	3686.10	3686.50	3691.36	3709.76
Photon detection	2.0								
Tracking	2.0								
Luminosity	1.0								
Helix parameter	0.6	0.6	0.5	0.5	0.5	0.6	0.4	0.5	0.6
Peaking background	1.9								
J/ψ veto	0.2	0.2	0.4	0.8	0.3	< 0.1	0.2	1.1	0.4
$\mathcal{B}(\eta \rightarrow \gamma\gamma)$	0.5								
MC modeling	0.1	0.8	1.1	0.4	0.1	0.3	0.1	0.2	< 0.1
Fit to $m_{\gamma\gamma}$	4.4	2.2	4.7	1.4	2.4	0.4	2.4	6.3	17.2
Total	5.7	4.3	6.0	4.0	4.4	3.7	4.3	7.4	17.6

complex coupling constants, quoted resonance parameters are smeared with their uncertainties. The difference of the detection efficiencies obtained with the new and nominal MC samples is taken as the uncertainty. The systematic uncertainty from the fit to the $m_{\gamma\gamma}$ spectrum is taken into account in two aspects. The uncertainty associated with the fit range is estimated by varying the fit range by 5 MeV. The uncertainty from the background shape is estimated by using a second-order polynomial in the fit. For each of these two effects, the difference between the signal yields obtained with nominal and alternative fit is taken as the corresponding systematic uncertainty. Adding these two items in quadrature, we obtain the combined systematic uncertainty from these two effects. The systematic uncertainty due to peaking background is estimated by studying inclusive MC sample. The systematic uncertainty due to the quoted branching fractions of $\mathcal{B}(\pi^0 \rightarrow \gamma\gamma)$ and $\mathcal{B}(\eta \rightarrow \gamma\gamma)$ are $< 0.1\%$ and 0.5% [3], respectively.

B. Uncertainties on intermediate resonance measurements

The systematic uncertainties on the intermediate resonance measurements are divided into two categories. The first one is non-PWA related, including photon detection, tracking efficiency of proton, helix parameter, normalization factor f_c , interference with continuum process, $\mathcal{B}(\pi^0 \rightarrow \gamma\gamma)$ or $\mathcal{B}(\eta \rightarrow \gamma\gamma)$, and the number of $\psi(3686)$. The overlapping uncertainties are estimated in the same way as in Sec. VI A.

The systematic uncertainty due to the normalization factor f_c is estimated by varying f_c within its uncertainty. The difference between signal yields obtained with nominal and alternative f_c is taken to be the uncertainty. The systematic uncertainty caused by an unknown phase angle between the $\psi(3686)$ resonance and continuum process is estimated by following Ref. [46]. The ratio of the maximum impact from the interference term with respect to the resonance term is defined as

$$r_R^{\max} = \frac{2}{\hbar c} AB \sin(\pi/2), A = \sqrt{\frac{\sigma_c}{\mathcal{B}}}. \quad (21)$$

Here, σ_c is the cross section of the continuum process $e^+e^- \rightarrow N^*\bar{p} + c.c. \rightarrow p\bar{p}\pi^0(\eta)$ and \mathcal{B} is the branching fraction of $\psi(3686) \rightarrow N^*\bar{p} + c.c. \rightarrow p\bar{p}\pi^0(\eta)$. The factor $B = M_{\psi(3686)}/\sqrt{12\pi\mathcal{B}(\psi(3686) \rightarrow e^+e^-)} = 6.74$ GeV is a constant depending on the $\psi(3686)$ resonance parameters. To be conservative, r_R^{\max} is taken to be the uncertainty. The systematic uncertainty on the total number of $\psi(3686)$ events is 0.5% .

The PWA related systematic uncertainties include the used mass and width, energy-dependent width parameters, the J/ψ veto requirement of $|M_{p\bar{p}} - 3.097| < 0.05$ GeV, hadronic background, and fit bias. The systematic uncertainty due to hadronic background is estimated by

rescaling the background level according to our study on the data sample. The systematic uncertainty related to extra resonance states is studied by adding N^* states with less experimental confirmation or higher spin, *i.e.* $N(1675)$, $N(1680)$, and $N(1700)$ for $\psi(3686) \rightarrow p\bar{p}\pi^0$ but none for $\psi(3686) \rightarrow p\bar{p}\eta$, into our solution. Although the statistical significance for each additional resonance is greater than 5σ , the corresponding fit fractions are all less than 3% . Therefore no additional resonances are included in the fit, but are accounted as sources of systematic uncertainty. The states with higher spin or weaker experimental confirmation are not considered in this work. The systematic uncertainty due to the energy-dependent width parameters is estimated by varying the branching fractions r_i in Table 1 within their individual uncertainties. For the above three sources, the maximum difference of signal yield obtained with the nominal and alternative fit is taken to be their uncertainty. The systematic uncertainty caused by the requirement of $|M_{p\bar{p}} - 3.097| < 0.05$ GeV is studied in the same way as in Sec. VI A. The systematic uncertainty due to the fixed masses and widths in the nominal fit, is estimated by varying the fixed values according to their uncertainties, shown in Table 2, within 3σ region, and repeating the fit. In total, 40 fits are performed with mass and width variations and the standard deviations of the measured branching fractions are taken as the associated systematic uncertainty. The systematic uncertainty due to fit bias is studied by performing an input/output check. Toy MC samples are generated according to the PWA fit result with simulated background events added. The same PWA fit is performed to each toy MC sample and the pull distributions of fitted signal yields are obtained. Any non-zero mean value of a pull distribution, indicating a possible fit bias, is taken as its uncertainty.

The systematic uncertainties for $\psi(3686) \rightarrow p\bar{p}\pi^0$ and $\psi(3686) \rightarrow p\bar{p}\eta$ are summarized in Tables 7 and 8, respectively.

VII. FIT TO OBSERVED CROSS SECTIONS

Least square fits are performed to the observed cross sections of $e^+e^- \rightarrow p\bar{p}\pi^0$ and $e^+e^- \rightarrow p\bar{p}\eta$ to obtain the branching fractions of $\psi(3686) \rightarrow p\bar{p}\pi^0$ and $\psi(3686) \rightarrow p\bar{p}\eta$, respectively.

The χ^2 is constructed as

$$\chi^2 = (\Delta\vec{\sigma})^T V^{-1} \Delta\vec{\sigma}, \quad (22)$$

where the difference in cross section $\Delta\vec{\sigma}_i = \sigma_i - \sigma_i^{\text{fit}}(\vec{\theta})$ and V is the covariance matrix. The σ_i and σ_i^{fit} are the measured and fitted values for cross section at the i -th energy point, respectively. The covariance matrix is constructed as $V_{ii} = \sigma_{\text{sta},i}^2 + \sigma_{\text{sys-corr},i}^2 + \sigma_{\text{sys-uncorr},i}^2 + (\sigma_{\text{beam},i} \times \frac{d\sigma_{\text{obs}}}{d\sqrt{s}})^2$ for diagonal elements and $V_{ij} = \sigma_{\text{sys-corr},i} \times \sigma_{\text{sys-corr},j}$ for off-diagonal elements ($i \neq j$). The $\sigma_{\text{sys-corr}}$ includes the systematic uncertainties of

Table 7. Relative systematic uncertainties of the branching fractions for intermediate resonance in $\psi(3686) \rightarrow p\bar{p}\pi^0$ (in percent).

Source	$N(940)$	$N(1440)$	$N(1520)$	$N(1535)$	$N(1650)$	$N(1710)$	$N(1720)$	$N(2100)$	$N(2300)$	$N(2570)$
Photon detection	2.0									
Tracking	2.0									
Helix parameter	0.6	0.7	0.6	0.5	0.5	0.6	0.7	0.5	0.6	0.5
Normalization factor f_c	< 0.1	< 0.1	0.1	< 0.1	< 0.1	0.1	< 0.1	< 0.1	0.2	0.1
Interference with continuum	5.2	9.1	24.9	8.0	11.9	20.3	12.8	17.4	34.0	23.7
$\mathcal{B}(\pi^0 \rightarrow \gamma\gamma)$	< 0.1									
Number of $\psi(3686)$	0.5									
Quoted mass and width	6.6	11.4	16.9	13.3	24.7	47.7	36.1	30.8	66.5	29.7
Extra resonance states	2.4	20.5	4.4	12.6	20.6	77.4	7.2	26.3	30.2	63.9
Energy-dependent width	1.3	5.5	0.7	3.9	1.8	10.2	1.3	1.1	6.2	1.4
Hadronic background	3.8	1.9	0.1	0.9	0.4	3.4	0.5	0.7	7.7	0.6
J/ψ veto	2.9	0.1	0.8	1.4	1.3	3.2	2.5	1.9	7.7	2.5
Fit bias	0.7	1.4	1.2	0.3	2.0	7.6	1.8	8.9	6.2	2.3
Total	10.5	26.0	30.6	20.6	34.6	94.2	39.2	45.1	81.8	74.5

Table 8. Relative systematic uncertainties of the branching fractions for $N(1535)$ and $N(1710)$ in $\psi(3686) \rightarrow p\bar{p}\eta$ (in percent).

Source	$N(1535)$	$N(1710)$
Photon detection	2.0	
Tracking	2.0	
Helix parameter	0.7	0.5
Normalization factor f_c	< 0.1	< 0.1
Interference with continuum	13.3	6.9
$\mathcal{B}(\eta \rightarrow \gamma\gamma)$	0.5	
Number of $\psi(3686)$	0.5	
Quoted mass and width	2.9	39.0
Extra resonance states	...	
Running width parameters	0.3	< 0.1
Hadronic background	0.5	1.2
J/ψ veto	0.7	0.4
Fit bias	0.7	4.8
Total	14.0	40.0

tracking, PID, and $\mathcal{B}(\pi^0 \rightarrow \gamma\gamma)$ or $\mathcal{B}(\eta \rightarrow \gamma\gamma)$. The $\sigma_{\text{beam},i} = 0.3$ MeV is the uncertainty on the beam energy.

The line shape of observed cross sections $\sigma_{\text{obs}}(s)$ is constructed as follows. The Born cross section is modeled with

$$\sigma_{\text{Born}} = |A_{\text{con}} + A_{\text{res}} \times e^{i\phi}|^2. \quad (23)$$

The continuum contributions $A_{\text{con}}(s) = a/s^n$ are fixed to those in Refs. [38] and [41] for π^0 and η channels, respectively. The A_{res} is defined as

$$A_{\text{res}}(s) = \frac{\sqrt{12\pi}\Gamma_{ee}\Gamma_{\text{tot}}\mathcal{B}_f}{s - M^2 + iM\Gamma_{\text{tot}}}. \quad (24)$$

Here, Γ_{ee} is the electronic partial width; Γ_{tot} is the total width; \mathcal{B}_f is the branching fraction of $\psi(3686) \rightarrow p\bar{p}\pi^0$ or $\psi(3686) \rightarrow p\bar{p}\eta$; M is the mass of $\psi(3686)$. In the fit, Γ_{tot} , and M are fixed to the PDG values [3]. The impact from ISR effect on the cross section is included by

$$\sigma'(s) = \int_{M_{\text{cut}}}^{\sqrt{s}} dm \frac{2m}{s} W(s, x) \sigma_{\text{Born}}(m), \quad (25)$$

where $W(s, x)$ is the radiative function up to $\mathcal{O}(\alpha^2)$ [39] and M_{cut} is set to be 3.65 GeV. This integration is performed in the same way as in Ref. [39]. The beam spread effect is considered by performing a Gaussian convolution to the cross section with

$$\sigma_{\text{obs}}(s) = \int ds' \sigma'(s) \frac{1}{\sqrt{2\pi}S_E} \exp\left(-\frac{(s-s')^2}{2S_E^2}\right), \quad (26)$$

where the S_E is the beam energy spread.

Figure 7 shows the fit results to $\psi(3686) \rightarrow p\bar{p}\pi^0$ and $\psi(3686) \rightarrow p\bar{p}\eta$. The fitted parameters and calculated branching fractions are summarized in Table 9.

VIII. RATIO OF $\Gamma_{N(1535) \rightarrow N\eta} / \Gamma_{N(1535) \rightarrow N\pi}$

The ratio of decay widths $\Gamma_{N(1535) \rightarrow N\eta} / \Gamma_{N(1535) \rightarrow N\pi}$ does not depend on whether $N(1535)\bar{p} + c.c.$ is from γ^* or $\psi(3686)$. Therefore, the systematic uncertainties from the interference between $\psi(3686)$ resonance and continuum process and normalization factor f_c , and some common terms, including photon detection, tracking, total number of $\psi(3686)$ events, and helix parameter, are ex-

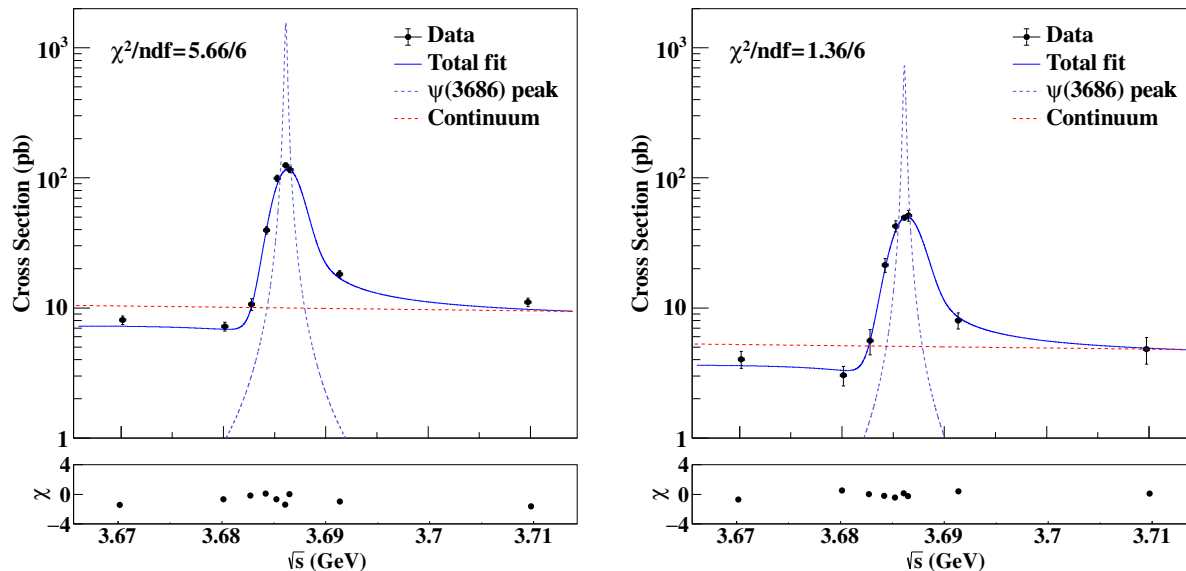


Fig. 7. Fit to the observed cross sections of (a) $\psi(3686) \rightarrow p\bar{p}\pi^0$ and (b) $\psi(3686) \rightarrow p\bar{p}\eta$ around the $\psi(3686)$ peak. Destructive solutions are shown as examples. The dots with error bars are data, the blue solid lines are the fit results, the cyan dashed lines are the $\psi(3686)$ peaks without beam spread effect, and the red dashed lines are the continuum processes.

Table 9. Fitted parameters of $\psi(3686) \rightarrow p\bar{p}\pi^0$ and $\psi(3686) \rightarrow p\bar{p}\eta$, and corresponding branching fractions \mathcal{B}_f . The first uncertainties include both statistical and systematic. The second uncertainties of \mathcal{B}_f are from $\Gamma_{ee} = (2.33 \pm 0.04)$ KeV [3].

$\psi(3686) \rightarrow p\bar{p}\pi^0$	$\mathcal{B}_f \Gamma_{ee} (0.1 \text{ eV})$	ϕ ($^\circ$)	ΔE (MeV)	$\mathcal{B}_f (\times 10^{-6})$
Constructive solution	3.12 ± 0.26	65.0 ± 6.7	1.27 ± 0.09	$133.9 \pm 11.2 \pm 2.3$
Destructive solution	4.28 ± 0.32	-68.9 ± 5.7	1.27 ± 0.09	$183.7 \pm 13.7 \pm 3.2$
$\psi(3686) \rightarrow p\bar{p}\eta$	$\mathcal{B}_f \Gamma_{ee} (0.1 \text{ eV})$	ϕ ($^\circ$)	ΔE (MeV)	$\mathcal{B}_f (\times 10^{-6})$
Constructive solution	1.44 ± 0.15	58.9 ± 14.1	1.39 ± 0.14	$61.5 \pm 6.5 \pm 1.1$
Destructive solution	1.98 ± 0.16	-63.8 ± 12.1	1.39 ± 0.14	$84.4 \pm 6.9 \pm 1.4$

pected to cancel in the ratio and are therefore excluded.

The ratio of the partial decay widths between $N(1535) \rightarrow N\eta$ and $N(1535) \rightarrow N\pi$ is calculated by

$$\frac{\Gamma_{N(1535) \rightarrow N\eta}}{\Gamma_{N(1535) \rightarrow N\pi}} = \frac{N_{\text{sig}}^\eta / (\epsilon^\eta \times \mathcal{B}(\eta \rightarrow \gamma\gamma))}{3 \times N_{\text{sig}}^{\pi^0} / (\epsilon^{\pi^0} \times \mathcal{B}(\pi^0 \rightarrow \gamma\gamma))}, \quad (27)$$

where the factor 3 includes both $p\pi^0$ and $n\pi^+ + c.c.$ contributions by assuming isospin conservation. Finally, $\Gamma_{N(1535) \rightarrow N\eta} / \Gamma_{N(1535) \rightarrow N\pi}$ is determined to be $0.99 \pm 0.05 \pm 0.19$, where the first uncertainty is statistical and the second one is systematic.

IX. SUMMARY

In summary, using a sample of $(2712 \pm 14) \times 10^6$ $\psi(3686)$ events collected with the BESIII detector, partial wave analyses of the decays $\psi(3686) \rightarrow p\bar{p}\pi^0$ and $\psi(3686) \rightarrow p\bar{p}\eta$ are performed. The data can be well described by considering several well-established N^* states.

Taking into account the interference effects in this analysis, the improved measurement on branching fractions of $\psi(3686) \rightarrow p\bar{p}\pi^0$ and $\psi(3686) \rightarrow p\bar{p}\eta$ are presented. The deviations from previous BESIII results [12, 13] are attributed mainly to the absence of consideration of interference effects in the previous measurements. Combining $\mathcal{B}(J/\psi \rightarrow p\bar{p}\pi^0)$ from the PDG [3], the ratio of $\mathcal{B}(\psi(3686) \rightarrow p\bar{p}\pi^0) / \mathcal{B}(J/\psi \rightarrow p\bar{p}\pi^0)$ is determined to be $(11.3 \pm 1.2)\%$ and $(15.4 \pm 1.6)\%$, for constructive and destructive interference, respectively. Combining $\mathcal{B}(J/\psi \rightarrow p\bar{p}\eta)$ from the PDG [3], the ratio of $\mathcal{B}(\psi(3686) \rightarrow p\bar{p}\eta) / \mathcal{B}(J/\psi \rightarrow p\bar{p}\eta)$ is determined to be $(3.1 \pm 0.4)\%$ and $(4.2 \pm 0.4)\%$, for constructive and destructive interferences, respectively. The “12% rule” [47–49] is significantly violated in the $p\bar{p}\eta$ final state but is confirmed in the $p\bar{p}\pi^0$ final state. The branching fractions of several N^* intermediate states are determined as well in this analysis.

The ratio of $\Gamma_{N(1535) \rightarrow N\eta} / \Gamma_{N(1535) \rightarrow N\pi}$ is determined to be $0.99 \pm 0.05 \pm 0.19$, which is consistent with $\Gamma_{N(1535) \rightarrow N\eta} / \Gamma_{N(1535) \rightarrow N\pi} = 1.00 \pm 0.40$ averaged by the

PDG [3] based on fixed-target experiment results and previous BESIII publications [12, 13], but with much improved precision. This result confirms the exotic property of $N(1535)$ in an e^+e^- collider experiment for the first time and suggests a strong $s\bar{s}$ component in $N(1535)$ [2].

X. ACKNOWLEDGMENTS

The BESIII collaboration thanks the staff of BEPCII and the IHEP computing center for their strong support. This work is supported in part by National Key R&D Program of China under Contracts Nos. 2020YFA0406300, 2020YFA0406400; National Natural Science Foundation of China (NSFC) under Contracts Nos. 12075252, 12175244, 11875262, 11635010, 11735014, 11835012, 11935015, 11935016, 11935018, 11961141012, 12022510, 12025502, 12035009, 12035013, 12192260, 12192261, 12192262, 12192263, 12192264, 12192265; the Chinese Academy of Sciences (CAS) Large-Scale Scientific Facility Program; Joint Large-Scale Scientific Facility Funds of the NSFC and CAS under Contract No. U1832207; CAS Key Research Program of Frontier Sciences under Contract No. QYZDJ-

SSW-SLH040; 100 Talents Program of CAS; INPAC and Shanghai Key Laboratory for Particle Physics and Cosmology; ERC under Contract No. 758462; European Union's Horizon 2020 research and innovation programme under Marie Skłodowska-Curie grant agreement under Contract No. 894790; German Research Foundation DFG under Contracts Nos. 443159800, Collaborative Research Center CRC 1044, GRK 2149; Istituto Nazionale di Fisica Nucleare, Italy; Ministry of Development of Turkey under Contract No. DPT2006K-120470; National Science and Technology fund; National Science Research and Innovation Fund (NSRF) via the Program Management Unit for Human Resources & Institutional Development, Research and Innovation under Contract No. B16F640076; STFC (United Kingdom); Suranaree University of Technology (SUT), Thailand Science Research and Innovation (TSRI), and National Science Research and Innovation Fund (NSRF) under Contract No. 160355; The Royal Society, UK under Contracts Nos. DH140054, DH160214; The Knut and Alice Wallenberg Foundation, Sweden, the Swedish Research Council, the Swedish Foundation for International Cooperation in Research and Higher Education (STINT); U. S. Department of Energy under Contract No. DE-FG02-05ER41374.

-
- [1] E. Klempt and J. M. Richard, *Rev. Mod. Phys.* **82**, 1095 (2010).
- [2] L. Olbrich, M. Zetyenyi, F. Giacosa *et al.*, *Phys. Rev. D* **97**, 014007 (2018).
- [3] R. L. Workman *et al.* (Particle Data Group), *Prog. Theor. Exp. Phys.* **2022**, 083C01 (2022).
- [4] N. Kaiser, P. B. Siegel, and W. Weise, *Phys. Lett. B* **362**, 23 (1995).
- [5] P. C. Bruns, M. Mai, and U. G. Meissner, *Phys. Lett. B* **697**, 254 (2011).
- [6] E. J. Garzon and E. Oset, *Phys. Rev. C* **91**, 025201 (2015).
- [7] C. S. An and B. S. Zou, *Sci. Sin. G* **52**, 1452 (2009).
- [8] B. C. Liu and B. S. Zou, *Phys. Rev. Lett.* **96**, 042002 (2006).
- [9] X. Cao, J. J. Xie, B. S. Zou *et al.*, *Phys. Rev. C* **80**, 025203 (2009).
- [10] Z. W. Liu, W. Kamleh, D. B. Leinweber *et al.*, *Phys. Rev. Lett.* **116**, 082004 (2016).
- [11] J. P. Alexander *et al.* (CLEO Collaboration), *Phys. Rev. D* **82**, 092002 (2010).
- [12] M. Ablikim *et al.* (BESIII Collaboration), *Phys. Rev. Lett.* **110**, 022001 (2013).
- [13] M. Ablikim *et al.* (BESIII Collaboration), *Phys. Rev. D* **88**, 032010 (2013).
- [14] M. Ablikim *et al.* (BESIII Collaboration), *Nucl. Instrum. Meth. A* **614**, 345 (2010).
- [15] C. H. Yu *et al.*, *Proceedings of IPAC 2016, Busan, Korea, 2016*.
- [16] M. Ablikim *et al.* (BESIII Collaboration), *Chin. Phys. C* **44**, 040001 (2020).
- [17] J. Lu, Y. Xiao, X. Ji, *Radiat. Detect. Technol. Methods* **4**, 337–344 (2020).
- [18] J. W. Zhang, L. H. Wu, S. S. Sun *et al.*, *Radiat. Detect. Technol. Methods* **6**, 289–293 (2022).
- [19] X. Li *et al.*, *Radiat. Detect. Technol. Methods* **1**, 13 (2017); Y. X. Guo *et al.*, *Radiat. Detect. Technol. Methods* **1**, 15 (2017); P. Cao *et al.*, *Nucl. Instrum. Meth. A* **953**, 163053 (2020).
- [20] S. Agostinelli *et al.* (GEANT4 Collaboration), *Nucl. Instrum. Meth. A* **506**, 250 (2003).
- [21] S. Jadach, B. F. L. Ward and Z. Was, *Phys. Rev. D* **63**, 113009 (2001); *Comput. Phys. Commun.* **130**, 260 (2000).
- [22] D. J. Lange, *Nucl. Instrum. Meth. A* **462**, 152 (2001); R. G. Ping, *Chin. Phys. C* **32**, 599 (2008).
- [23] J. C. Chen, G. S. Huang, X. R. Qi, D. H. Zhang and Y. S. Zhu, *Phys. Rev. D* **62**, 034003 (2000); R. L. Yang, R. G. Ping and H. Chen, *Chin. Phys. Lett.* **31**, 061301 (2014).
- [24] J. X. Wang, *Nucl. Instrum. Meth. A* **534**, 241 (2004).
- [25] B. C. Hunt and D. M. Manley, *Phys. Rev. C* **99**, 055205 (2019).
- [26] F. V. Hippel and C. Quigg, *Phys. Rev. D* **5**, 624 (1972).
- [27] E. M. Aitala *et al.* (Fermilab E791 collaboration), *Phys. Rev. Lett.* **86**, 770 (2001).
- [28] G. J. Gounaris and J. J. Sakurai, *Phys. Rev. Lett.* **21**, 244 (1968).
- [29] F. James and M. Roos, *Comput. Phys. Commun.* **10**, 343(1975).
- [30] M. Ablikim *et al.* (BES Collaboration), *Phys. Rev. Lett.* **97**, 062001 (2006).
- [31] R. Sinha and S. Okubo, *Phys. Rev. D* **20** 2333 (1984).
- [32] W. H. Liang, P. N. Shen, B. S. Zou *et al.*, *Eur. Phys. J. A* **21**, 487 (2004).
- [33] M. Ablikim *et al.* (BES Collaboration), *Phys. Rev. D* **80**, 052004 (2009).

- [34] B. Aubert *et al.*, [Phys. Rev. D **73**, 052003 \(2006\)](#).
- [35] M. Ablikim *et al.* (BESIII Collaboration), [Phys. Rev. D **100**, 032004 \(2019\)](#).
- [36] J. P. Lees *et al.* (BaBar Collaboration), [Phys. Rev. D **86**, 032013 \(2012\)](#).
- [37] A. V. Anisovich *et al.*, [Phys. Lett. B **542**, 8 \(2002\)](#).
- [38] Y. Q. Wang and C. Z. Yuan, [Phys. Rev. D **106**, 054014 \(2022\)](#).
- [39] R. G. Ping, [Chin. Phys. C **38**, 083001\(2014\)](#)
- [40] A. V. Anisovich *et al.*, [Phys. Lett. B **542**, 19 \(2002\)](#).
- [41] M. Ablikim *et al.* (BESIII Collaboration), [Phys. Rev. D **104**, 092008 \(2021\)](#).
- [42] M. Ablikim *et al.* (BESIII Collaboration), [Chin. Phys. C **39**, 093001 \(2015\)](#).
- [43] M. Ablikim *et al.* (BESIII Collaboration), [Phys. Rev. D **87**, 012007 \(2013\)](#).
- [44] M. Ablikim *et al.* (BESIII Collaboration), [Phys. Rev. D **87**, 052005 \(2010\)](#).
- [45] M. Ablikim *et al.* (BESIII Collaboration), [Phys. Rev. D **87**, 012002 \(2013\)](#).
- [46] Y. P. Guo and C. Z. Yuan, [Phys. Rev. D **105**, 114001 \(2022\)](#).
- [47] T. Appelquist and H. D. Politzer, [Phys. Rev. Lett. **34**, 43 \(1975\)](#).
- [48] A. De Rujula, [Phys. Rev. Lett. **34**, 46 \(1975\)](#).
- [49] N. Brambilla, S. Eidelman, B. K. Heltsley *et al.*, [Eur. Phys. J. C **71**, 1534 \(2011\)](#).
- [50] B. S. Zou, [Nucl. Phys. A **827**, 333C-335C \(2009\)](#).